

# Supporting Information

## **Tailoring Synthetic Polypeptide Design for Directed Fibril Superstructure Formation and Enhanced Hydrogel Properties**

Tianjian Yang<sup>a†</sup>, Tianrui Xue<sup>c†</sup>, Jianan Mao<sup>b</sup>, Yingying Chen<sup>d</sup>, Huidi Tian<sup>b</sup>, Arlene Bartolome<sup>b</sup>,  
Hongwei Xia<sup>b</sup>, Xudong Yao<sup>b</sup>, Challa V. Kumar<sup>b</sup>, Jianjun Cheng<sup>cd\*</sup>, Yao Lin<sup>ab\*</sup>

<sup>a</sup>*Polymer Program, Institute of Materials Science, University of Connecticut, Storrs, CT 06269, USA.*

<sup>b</sup>*Department of Chemistry, University of Connecticut, Storrs, CT 06269, USA.*

<sup>c</sup>*Department of Chemistry, University of Illinois at Urbana-Champaign, Urbana, IL 61801, USA.*

<sup>d</sup>*Department of Materials Science and Engineering, University of Illinois at Urbana-Champaign, Urbana, IL 61801, USA*

<sup>†</sup>*Tianjian Yang and Tianrui Xue contributed equally to this work.*

*\*Corresponding authors.*

Email: [yao.lin@uconn.edu](mailto:yao.lin@uconn.edu) (Y.L.) or [jianjunc@illinois.edu](mailto:jianjunc@illinois.edu) (J.C.)

## Table of Contents

<b>1. Materials and methods</b> .....	3
1.1 Materials.....	3
1.2 Nuclear magnetic resonance (NMR).....	4
1.3 Gel permeation chromatography (GPC).....	4
1.4 NCA copolymerization kinetics by high performance liquid chromatography (HPLC).....	4
1.5 Circular dichroism (CD) spectra.....	5
1.6 Fourier transform infrared (FTIR) spectra.....	5
1.7 Small-angle X-ray scattering (SAXS) and wide-angle X-ray scattering (WAXS).....	5
1.8 ThT-based fluorescence kinetic assays by microplate reader.....	6
1.9 Transmission electron microscopy (TEM) and negatively stained TEM.....	6
1.10 Scanning electron microscope (SEM) and critical point dryer.....	6
1.11 Rheology.....	7
<b>2. Experimental Section</b> .....	8
2.1 Synthesis of <i>O</i> -benzyl-L-Serine NCA (BLS-NCA).....	8
2.2 Synthesis of <i>O</i> -benzyl-L-tyrosine NCA (BLT-NCA).....	8
2.3 Synthesis of copolypeptides with leucine, alanine, valine and tyrosine.....	8
2.4 Synthesis of Copolypeptides with serine <i>via</i> SIMPLE Polymerization method.....	9
2.5 Synthesis of Copolypeptides with three components with crown ether (CE) as catalyst.....	9
2.6 Determination of the Randomness of Amino Acids in the Copolypeptides by NCA ROP Copolymerization Kinetics.....	10
2.7 Supramolecular Assembly of Copolypeptides in Dilute Solutions.....	10
2.8 Supramolecular Hydrogelation of Copolypeptides.....	11
2.9 Supramolecular Assembly Kinetics of Copolypeptides monitored by in-situ ThT fluorescence assays.....	11
2.10 Supramolecular Assembly Kinetic Data Processing.....	12
2.11 Analysis of the Supramolecular Assembly Kinetics.....	12
2.12 Statistics of the length and width of supramolecular assemblies.....	12
<b>3. Supplementary Figures</b> .....	13
<b>4. Supplementary Tables</b> .....	47
<b>5. NMR spectra</b> .....	49
<b>6. References</b> .....	63

## 1. Materials and methods

### 1.1 Materials.

All chemicals were purchased from MilliporeSigma (Burlington, MA, USA) unless otherwise specified. Amino acids were purchased from Chem-Impex International Inc. (Wood Dale, IL, USA). Deuterated solvents were purchased from Cambridge Isotope Laboratories, Inc. (Tewksbury, MA, USA). Methoxy poly(ethylene glycol) amine (mPEG-NH<sub>2</sub>  $M_n = 550$  Da, DP = 12) was purchased from Laysan Bio, Inc. (Arab, AL, USA). Anhydrous *N,N*-dimethylformamide (DMF) was treated with polymer bound isocyanates (MilliporeSigma, St. Louis, MO, USA) to remove any amine residues and was stored at room temperature. Anhydrous tetrahydrofuran (THF) and dichloromethane (DCM) were obtained from a solvent purification system and were stored over 3 Å molecular sieves before being used.  $\gamma$ -Benzyl-L-glutamate *N*-carboxyanhydride (BLG-NCA),<sup>1</sup> L-leucine NCA (Leu-NCA),<sup>2</sup> L-alanine NCA (Ala-NCA),<sup>3</sup> and L-Valine NCA (Val-NCA)<sup>4</sup> were synthesized according to the literature procedures without further purification. The wide-pH range buffer containing boric acid, citric acid, and sodium phosphate as active species (BCP buffer) was prepared according to the previous report.<sup>1</sup> Iodotrimethylsilane (TMSI) was purchased from Oakwood (Estill, SC, USA). Deionized (DI) water was generated by a Milli-Q direct water purification system (MilliporeSigma, Burlington, MA, USA). Sodium acetate buffer, hydrochloric acid (HCl), and sodium hydroxide (NaOH) were purchased from Sigma-Aldrich (Milwaukee, WI, USA). Thioflavin T (ThT) was obtained from Biotium (Fremont, CA, USA). 0.45  $\mu$ m Nylon and PTFE syringe filters were purchased from GE Healthcare (Chicago, IL, USA). Centrifugal filter units with regenerated cellulose membranes (MWCO = 3000 Da) were purchased from MilliporeSigma (Burlington, MA, USA). Dialysis tubes (MWCO = 3500 Da) were purchased from Spectrum Chemical (New Brunswick, NJ, USA). 96-well half-area, clear bottom, and non-binding microplates and microplate sealing tapes were purchased from Corning (Corning, NY, USA). Centrifuge tubes were purchased from Corning (Corning, NY, USA). Microcentrifuge tubes were obtained from Eppendorf (Hamburg, Germany).

## **1.2 Nuclear magnetic resonance (NMR).**

NMR spectra were recorded on a DMX 500 MHz spectrometer (Bruker Corporation, Billerica, MA, USA). <sup>1</sup>H NMR spectrum of the copolypeptides were carried out in CDCl<sub>3</sub>/TFA-*d* (70:30, v/v). Chemical shifts were referenced to the residual protons of deuterated solvents and reported in ppm. MestReNova (version 14.2.1, Mestrelab Research, Escondido, CA, USA) was used in the analysis of NMR data.

## **1.3 Gel permeation chromatography (GPC).**

Gel permeation chromatography (GPC) data was collected *via* an instrument equipped with an isocratic pump (1260 Infinity II, Agilent, Santa Clara, CA, USA), a multi-angle static light scattering (MALS) detector with the detection wavelength at 658 nm (DAWN HELEOS-II, Wyatt Technology, Santa Barbara, CA, USA), and a differential refractometer (dRI) detector (Optilab T-rEX, Wyatt Technology, Santa Barbara, CA, USA). Separations were performed by serially connected size exclusion columns (three PLgel MIXED-B columns, 10 μm, 7.5 × 300 mm, Agilent, Santa Clara, CA, USA) which were maintained at 40 °C using DMF containing 0.1 M LiBr as the mobile phase at a flow rate of 0.7 mL/min. The MALS detector was calibrated using pure toluene and then was used for the determination of the absolute molecular weights (MWs). All sample solutions were filtered by 0.45 μm PTFE filters before injection. The MWs of polypeptides were determined based on the *dn/dc* value of each sample calculated offline by using the internal calibration system processed by the software ASTRA 7 (version 7.1.3.15, Wyatt Technology, Santa Barbara, CA, USA).

## **1.4 NCA copolymerization kinetics by high performance liquid chromatography (HPLC).**

HPLC profiles for the aliquots of the copolymerization reaction were collected using a Shimadzu HPLC system which is comprised of a binary pump (SPD-10ADvp Micro Plunger Pump, SpectraLab, Markham, ON, Canada), a UV-Vis detector (SPD-10AVvp, SpectraLab, Markham, ON, Canada) that uses deuterium

lamp, and an oven (CTO-10Avp, SpectraLab, Markham, ON, Canada). A gradient changed mobile phase with water and acetonitrile was used at a flow rate of 1 mL/min. The oven temperature was set to 40 °C, and the UV absorbance of the mobile phase was used for the detection of the analytes.

### **1.5 Circular dichroism (CD) spectra.**

CD spectra were measured by a Chirascan V100 spectropolarimeter (Applied Photophysics, Leatherhead, Surrey, UK) using quartz cuvettes with either 0.5 mm, 1 mm, or 3 mm pathlength. The solution temperature was controlled by a Peltier holder.

### **1.6 Fourier transform infrared (FTIR) spectra.**

Attenuated total reflection infrared spectroscopy (FTIR-ATR) was carried out using a NICOLET MAGNA 560 spectrometer equipped with a diamond ATR element (ThermoFisher Sci., Waltham, MA, USA). Transmission infrared spectroscopy (FTIR) was carried out using a NICOLET MAGNA 560 spectrometer using a KBr plate (Sigma-Aldrich, Milwaukee, WI, USA). IR spectra were obtained with 4 cm<sup>-1</sup> resolution and 64 co-averages.

### **1.7 Small-angle X-ray scattering (SAXS) and wide-angle X-ray scattering (WAXS).**

SAXS and WAXS experiments were conducted simultaneously using the 16ID-LiX Beamline at the National Synchrotron Light Source II where is located at the Brookhaven National Laboratory (Upton, New York). The standard flow-cell-based solution scattering was set up, and the X-ray energy was 13.5 keV. The intensity is expressed as a function of scattering vector,  $q$  defined as  $\frac{4\pi}{\lambda} \sin \frac{\theta}{2}$ , where  $\theta$  is the scattering angle and  $\lambda$  is the wavelength. The data covers a  $q$  range from 0.005 to 2.5 Å<sup>-1</sup>. Radial averaging and  $q$ -conversion

of data were analyzed by using Jupyter Notebook.<sup>5</sup> The background subtraction and transmission correction were performed to minimize the intensity of the hydrogen bond from water at  $\sim 2.0 \text{ \AA}^{-1}$ .

### **1.8 ThT-based fluorescence kinetic assays by microplate reader.**

ThT-based fluorescence kinetic assays were performed using a FlexStation 3 microplate reader (Molecular Devices, San Jose, CA, USA). The pH values of solutions were measured by Orion 8103BNUWP ROSS Ultra pH Electrode (ThermoFisher Sci., Waltham, MA, USA) and adjusted to the targeted values.

### **1.9 Transmission electron microscopy (TEM) and negatively stained TEM.**

Morphologies of the supramolecular assemblies were characterized by a Tecnai T12 G2 Spirit BioTWIN (ThermoFisher Sci., Waltham, MA, USA) TEM operating at an accelerating voltage of 80 kV. Sample solutions were deposited on carbon film coated TEM grids, blotted by filter paper, and allowed to dry under ambient condition. For negatively stained samples, the sample solutions loaded on TEM grids were rinsed by 50  $\mu\text{L}$  of 0.5 wt% uranyl acetate solution and then blotted by filter paper followed by drying under ambient condition. The carbon-coated copper grids (carbon film 200 mesh copper, Ted Pella Inc., Redding, CA, USA) were pre-treated with plasma for 15s (Harrick Plasma PDC-32G, Harrick Plasma, Ithaca, NY, USA) before loading all the samples.

### **1.10 Scanning electron microscope (SEM) and critical point dryer.**

Morphologies of the supramolecular hydrogels were characterized by a FEI Nova NanoSEM 450 (Thermo Fisher Sci., Waltham, MA, USA) field emission SEM with an accelerating voltage of 2 kV and a stage bias of 500 V. Hydrogel samples were loaded into metal mesh critical point drying sample baskets (Ted Pella Inc., Redding, CA, USA) and then dehydrated in a series of ethanol-water mixtures with increasing ethanol

concentration from 20-100%, ending with a final immersion in 100% ethanol for overnight. Ethanol was removed at the supercritical point of CO<sub>2</sub> using a critical point dryer (Tousimis 931. GL, Rockville, MD, USA). Dehydrated samples were mounted on aluminum stubs using carbon tapes, and then coated with 15 nm of gold-palladium before imaging (Safematic CCU-010, Zizers, Switzerland). The actual gold-palladium thickness on the fibrous assemblies was lower than 15 nm as the surface area of nanostructured sample was much higher than a flat surface.

### **1.11 Rheology.**

Rheological measurements were performed using a Discovery HR30 rheometer (TA Instruments, New Castle, DE, USA). Hydrogels were loaded onto the stage and incubated for 2 min before all the measurements. A 20-mm aluminum parallel plate with water trap was used, and the gap height was set to 500  $\mu\text{m}$ . Temperature of hydrogels was controlled at 25  $^{\circ}\text{C}$  by the Peltier system. Water evaporation was prevented by a water trap. Each measurement was repeated multiple times using different batches of copolypeptide hydrogels. For strain sweep oscillatory rheology, strain from 0.1% to 1000% was applied at a frequency of 1.0 rad/s. For frequency sweep oscillatory rheology, frequency of 100  $\text{rad s}^{-1}$  to 0.1  $\text{rad s}^{-1}$  was applied at strain of 0.5%. To test the self-healing property of hydrogels, alternating strain (0.5% or 500%) with a fixed frequency of 1  $\text{rad s}^{-1}$  were applied.

## **2. Experimental section.**

### **2.1 Synthesis of *O*-benzyl-L-Serine NCA (BLS-NCA).**

BLS-NCA was synthesized according to a modified procedure from previously reported.<sup>6</sup> BLS (5.0 g, 25.6 mmol, 1 equiv.) was added into a flame-dried Schlenk flask, and the amino acid was dried under vacuum for 2 h. Anhydrous THF (75 mL) was then added into the flask, and the flask was cooled down to 0 °C with an ice bath. Phosgene solution (15 wt% in toluene, 36.6 mL, 51.2 mmol of phosgene, 2 equiv.) was added, and the mixture was stirred at 50 °C for 2 h. After the solution was cooled down to room temperature, solvent was removed under vacuum. (Note that phosgene is extremely toxic and should be handled with care. The residues in the cold trap need to be neutralized with saturated aqueous solution of NaHCO<sub>3</sub>.) The crude product was recrystallized three times at room temperature from anhydrous DCM/hexane (1:20, v/v). The product BLS-NCA was obtained as white needle-like crystals after drying under vacuum, and stored in a glove box at -30 °C. Isolated yield was 85 to 90%.

### **2.2 Synthesis of *O*-benzyl-L-tyrosine NCA (BLT-NCA).**

BLT-NCA was synthesized according to a modified procedure from previously reported.<sup>7</sup> BLT (10.0 g, 36.9 mmol, 1 equiv.) was added into a flame-dried Schlenk flask, and the amino acid was dried under vacuum for 2 h. Anhydrous THF (150 mL) was then added into the flask, and the flask was cooled down to 0 °C with an ice bath. Phosgene solution (15 wt% in toluene, 45.0 mL, 63.0 mmol of phosgene, 1.7 equiv.) was added, and the mixture was stirred at 50 °C for 4 h. After the solution was cooled down to room temperature, solvent was removed under vacuum. The crude product was recrystallized three times at room temperature from anhydrous THF/hexane (1:10, v/v). The product BLT-NCA was obtained as white needle-like crystals after drying under vacuum, and stored in a glove box at -30 °C. Isolated yield was 75 to 85%.

### **2.3 Synthesis of copolypeptides with leucine, alanine, valine and tyrosine.**

Poly( $\gamma$ -benzyl-L-glutamate) (PBLG), BLG-leucine based copolypeptides P(BLG<sub>x-co</sub>-Leu<sub>1-x</sub>)<sub>100</sub>, and BLG-alanine based copolypeptides P(BLG<sub>x-co</sub>-Ala<sub>1-x</sub>)<sub>100</sub> with a series of compositions were synthesized from DMF phase using hexylamine as initiator using previously reported methods.<sup>8</sup> BLG-valine based copolypeptides P(BLG<sub>x-co</sub>-Val<sub>1-x</sub>)<sub>100</sub>, and BLG-BLT based copolypeptides P(BLG<sub>x-co</sub>-BLT<sub>1-x</sub>)<sub>100</sub> with a series of compositions were synthesized from DCM phase using hexylamine as initiator using previously reported methods.<sup>9-10</sup> After the full conversion of monomers as confirmed by FTIR, the resulting polymer solution was filtered by 0.45  $\mu$ m PTFE filters, purified by precipitation in hexane/ether (1:1, v/v), and dried under vacuum. The deprotection of copolypeptides was done by TMSI in DCM. In a typical experiment, PBLG (80 mg, 0.36 mmol benzyl groups) was dissolved in DCM at room temperature, into which fresh TMSI (312  $\mu$ L, 2.19 mmol) was added. The solution was stirred at room temperature for 24 h and then at 40 °C for 24 h. After precipitation by the addition of hexane/ether (1:1, v/v) (40 mL), NaHCO<sub>3</sub> saturated solution (4 mL) was added to dissolve the solid residue. The aqueous phase was extracted by ether (3  $\times$  3 mL). The product polypeptide was purified by dialysis (MWCO = 3500 Da) for 48 h, filtered by 0.45  $\mu$ m Nylon filters, and lyophilized to give polypeptide in almost quantitative yield.

#### **2.4 Synthesis of Copolypeptides with serine *via* SIMPLE polymerization method.**

The glutamate-serine based copolypeptides P(Glu<sub>x-co</sub>-Ser<sub>1-x</sub>)<sub>200</sub> with a series of compositions were synthesized using a PEG-*b*-PBLG-NH<sub>2</sub> macroinitiator from SIMPLE polymerization method.<sup>1,11</sup> Typically, a w/o emulsion containing PEG-PBLG macroinitiators (1 mM) was prepared by emulsifying a mixture of a regular DCM solution of PEG-PBLG macroinitiators and an aqueous buffer (pH = 7.0, 2 wt%). NCAs were dissolved in regular DCM (0.1M), mixed with aqueous buffer (pH = 7.0, 18 wt%), and vortexed for 10 s. The w/o emulsion containing PEG-PBLG was then immediately added into the mixture to start the polymerization. Final condition was [M]<sub>0</sub> = 40 mM, [I]<sub>0</sub> = 0.2 mM, water:DCM = 1:10, w/w. After the full conversion of monomers as confirmed by FTIR, the resulting polymer solution was filtered by 0.45  $\mu$ m

PTFE filters, purified by precipitation in hexane/ether (1:1, v/v), and dried under vacuum. The deprotection of copolypeptides was similar with the above procedures.

### **2.5 Synthesis of Copolypeptides with three components with crown ether (CE) as catalyst.**

The glutamate-alanine-valine based copolypeptides  $P(\text{Glu}_x\text{-co-Ala}_y\text{-co-Val}_{1-x-y})_{200}$  with a series of compositions were synthesized using a PEG-PBLG-NH<sub>2</sub> macroinitiator from crown ether (CE) catalyzed polymerization method.<sup>12</sup> Typically, the DCM solution of CE 18-crown-6 (18-C-6) and NCAs were mixed, followed by the addition of PEG-PBLG macromolecular initiators. Final condition was  $[\text{M}]_0 = 100 \text{ mM}$ ,  $[\text{I}]_0 = 0.5 \text{ mM}$ ,  $[\text{CE}]_0 = 0.5 \text{ mM}$ . After the full conversion of monomers as confirmed by FTIR, the resulting polymer solution was filtered by 0.45  $\mu\text{m}$  PTFE filters, purified by precipitation in hexane/ether (1:1, v/v), and dried under vacuum. The deprotection of copolypeptides was similar with the above procedures.

### **2.6 Determination of the Randomness of Amino Acids in the Copolypeptides by NCA ROP Copolymerization Kinetics**

The copolymerization kinetic profiles were constructed using previously reported methods.<sup>11, 13</sup> At selected time during the copolymerization, aliquots (10  $\mu\text{L}$ ) were drawn from the reaction mixture and quenched by water/acetonitrile solvent (990  $\mu\text{L}$ , 1:1, v/v) immediately. Samples were placed for 24 h and then filtered by centrifugal filter units before being analyzed by HPLC (calibration curve in Figure S9a and S9b) for the conversion of various NCAs at different time points.

### **2.7 Supramolecular Assembly of Copolypeptides in Dilute Solutions.**

PGlu or PGlu-based copolypeptides were dissolved in MilliQ water or a 15 mM acetate buffer at a concentration of 1 mg/mL, yielding transparent solutions. For the kinetic studies, we utilized a 15 mM

acetate buffer to maintain consistent ionic strength with minimal variation. During TEM sample preparation, MilliQ water was employed to optimize imaging quality. The supramolecular assembly was initiated by firstly adjusting the solution pH to 4.0 using HCl with frequent vortex and then incubating at 45 °C.

## **2.8 Supramolecular Hydrogelation of Copolypeptides.**

Copolypeptides were first dissolved in MilliQ water to yield transparent polymer solution at a concentration of 20 mg/mL or 40 mg/mL. The solution pH was tuned to 4.2 by slowly adding 4 M HCl with frequent vortex. Supramolecular assembly of various copolypeptides was initiated by incubating the solutions at 45 °C and the resulting hydrogel was allowed to equilibrate at 45 °C overnight.

## **2.9 Supramolecular Assembly Kinetics of Copolypeptides monitored by *in-situ* ThT fluorescence assays.**

In a typical experiment, PLG (4 mg/mL, 0.53 mM), and ThT (500 μM) stock solutions were prepared in a filtered (0.22 μm Nylon syringe filter) 15 mM sodium acetate buffer. The pH of stock solutions was tuned to 4.0 using 1 M HCl. The reaction solutions were prepared by combining appropriate volumes of the stock solutions and diluting with a 15 mM sodium acetate buffer, pH 4.0, in low-binding Eppendorf tubes on ice. Each reaction solution also contained 50 μM of ThT as the *in-situ* fluorescent probe. Samples were pipetted into multiple wells of a Corning 3881 microplate, 100 μL per well. Each kinetic group was prepared and measured at least in triplicate. The microplates were sealed by Corning 6575 optical adhesive tapes, and the supramolecular polymerization was initiated by placing the microplate at 45 °C quiescent in a FLEXstation 3 plate reader. The supramolecular assembly kinetics were monitored by recording the ThT fluorescence every 45 min, through the bottom reading mode with 440 nm excitation, 490 nm emission, and 455 nm cutoff filter. The error bars in the kinetic profiles are smaller than the size of symbols.

### **2.10 Supramolecular Assembly Kinetic Data Processing.**

The calibration experiments performed in our previous studies showed show an excellent linear correlation between the ThT fluorescence and the mass concentration of PLG<sub>50</sub> amyloid fibrils.<sup>14</sup> To calculate the value of normalized assembly mass (fraction aggregated) at a given time, fluorescence intensities at 490 nm for each sampling point in a kinetic trace were normalized by the final fluorescence intensity at equilibrium. All the kinetic profiles are from the average of three independent experiments, showing a good reproducibility of the measurements.

### **2.11 Analysis of the Supramolecular Assembly Kinetics.**

The early-stage experimental ThT kinetic profiles with up to 15-20% of the normalized assembly mass were fitted in the AmyloFit 2.0 web software.<sup>15</sup> The values of critical nucleus sizes and effective rate constants were obtained using the global fitting method based on the secondary nucleation model.

### **2.12 Statistics of the length and width of supramolecular assemblies.**

The length and width of the supramolecular single fibers and fiber bundles were manually measured over 100 assemblies from the TEM images to reduce subjectivity. The measurements were performed using ImageJ. The aspect ratio values of various copolypeptide assemblies were calculated from dividing the fiber length by fiber width.

### 3. Supplementary Figures.

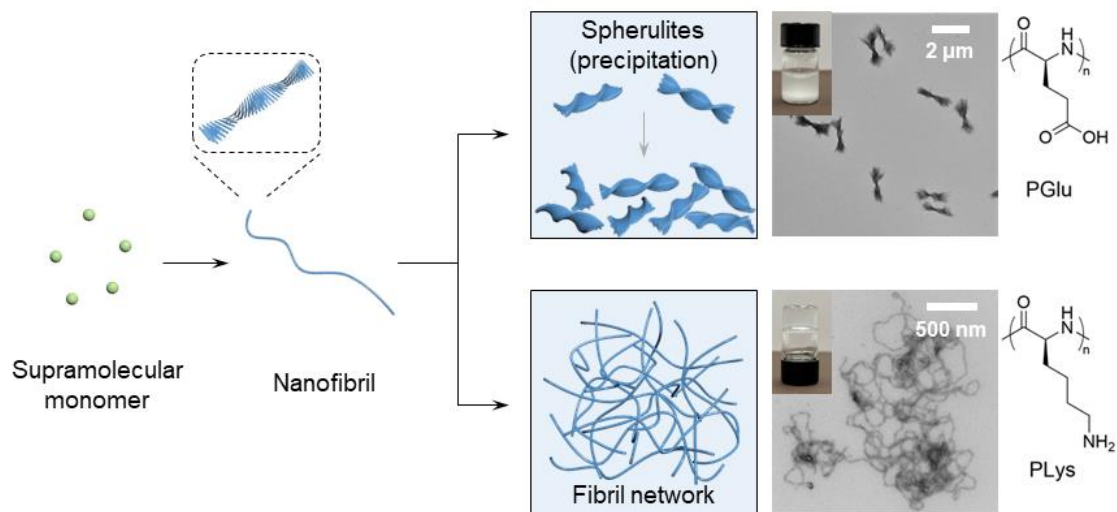


**Figure S1.** Schematic illustration of the supramolecular assembly and hydrogelation pathways from synthetic homo-polypeptides.

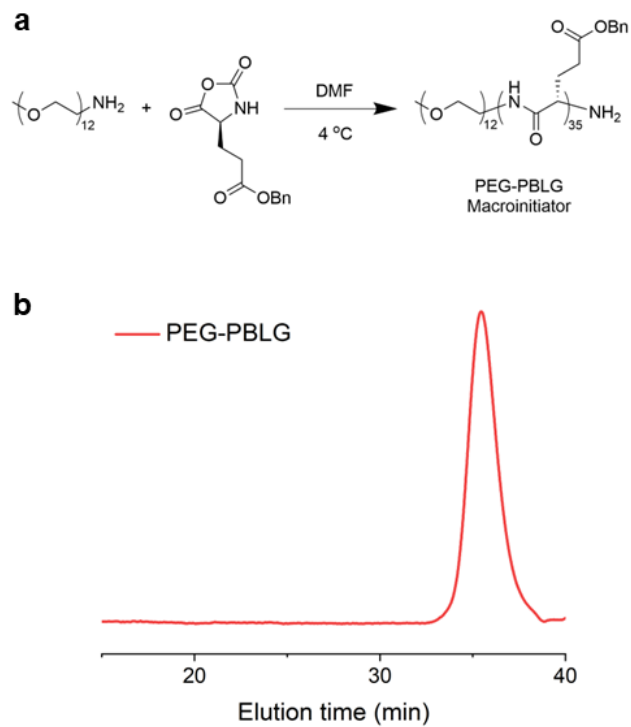


**Figure S2.** Characterization of PEG-PBLG macroinitiator. (a) Synthetic route to PEG-PBLG. (b) Normalized GPC-LS trace of PEG-PBLG ( $M_n = 8.3$  kDa,  $D = 1.05$ , DP for PBLG = 35).

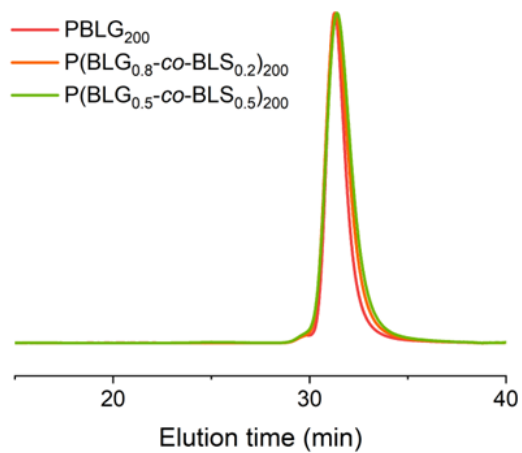


**Figure S3.** Characterization of BLG/BLS-based copolypeptides synthesized from SIMPLE copolymerization initiated by PEG-PBLG. Normalized GPC-LS trace of the resulting PEG-polypeptide with PBLG<sub>200</sub> ( $M_n = 48.3$  kDa,  $\mathcal{D} = 1.05$ ), PEG-polypeptide with P(BLG<sub>0.8</sub>-co-BLS<sub>0.2</sub>)<sub>200</sub> ( $M_n = 46.3$  kDa,  $\mathcal{D} = 1.05$ ), and PEG-polypeptide with P(BLG<sub>0.5</sub>-co-BLS<sub>0.5</sub>)<sub>200</sub> ( $M_n = 45.2$  kDa,  $\mathcal{D} = 1.05$ ). The PEG segment was decomposed after deprotection by TMSI.

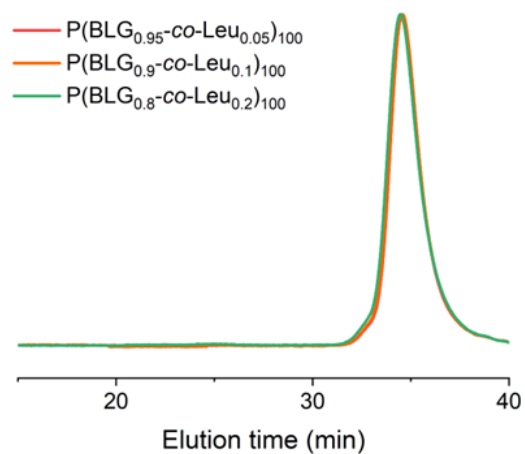


**Figure S4.** Characterization of  $P(\text{BLG}_{1-x}\text{-co-Leu}_x)_n$  synthesized from DMF phase copolymerization initiated by hexylamine. Normalized GPC-LS trace of resulting  $P(\text{BLG}_{0.95}\text{-co-Leu}_{0.05})_{100}$  ( $M_n = 19.2$  kDa,  $\mathcal{D} = 1.05$ ),  $P(\text{BLG}_{0.9}\text{-co-Leu}_{0.1})_{100}$  ( $M_n = 19.0$  kDa,  $\mathcal{D} = 1.05$ ), and  $P(\text{BLG}_{0.8}\text{-co-Leu}_{0.2})_{100}$  ( $M_n = 19.3$  kDa,  $\mathcal{D} = 1.05$ ).

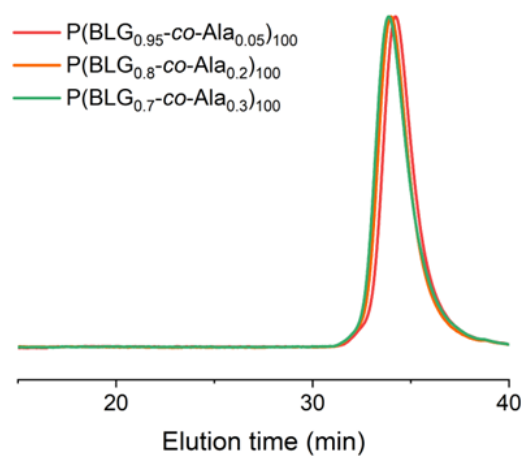


**Figure S5.** Characterization of  $P(\text{BLG}_{1-x}\text{-co-Ala}_x)_n$  synthesized from DMF phase copolymerization initiated by hexylamine. Normalized GPC-LS trace of resulting  $P(\text{BLG}_{0.95}\text{-co-Ala}_{0.05})_{100}$  ( $M_n = 17.6$  kDa,  $\mathcal{D} = 1.05$ ),  $P(\text{BLG}_{0.8}\text{-co-Ala}_{0.2})_{100}$  ( $M_n = 18.1$  kDa,  $\mathcal{D} = 1.08$ ), and  $P(\text{BLG}_{0.7}\text{-co-Ala}_{0.3})_{100}$  ( $M_n = 16.9$  kDa,  $\mathcal{D} = 1.07$ ).

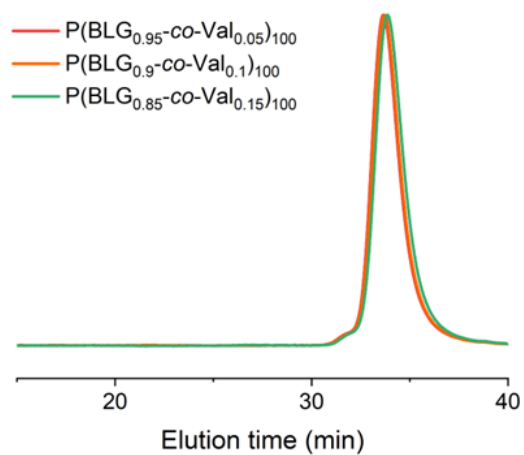


**Figure S6.** Characterization of  $P(\text{BLG}_{1-x}\text{-co-Val}_x)_n$  synthesized from DCM phase copolymerization initiated by hexylamine. Normalized GPC-LS trace of resulting  $P(\text{BLG}_{0.95}\text{-co-Val}_{0.05})_{100}$  ( $M_n = 19.5$  kDa,  $\mathcal{D} = 1.05$ ),  $P(\text{BLG}_{0.9}\text{-co-Val}_{0.1})_{100}$  ( $M_n = 18.5$  kDa,  $\mathcal{D} = 1.05$ ), and  $P(\text{BLG}_{0.85}\text{-co-Val}_{0.15})_{100}$  ( $M_n = 17.4$  kDa,  $\mathcal{D} = 1.05$ ).

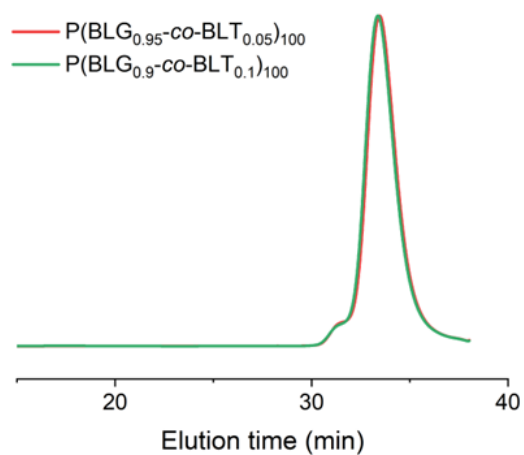


**Figure S7.** Characterization of  $P(\text{BLG}_{1-x}\text{-co-BLT}_x)_n$  synthesized from DCM phase copolymerization initiated by hexylamine. Normalized GPC-dRI trace of resulting  $P(\text{BLG}_{0.95}\text{-co-BLT}_{0.05})_{100}$  ( $M_n = 22.5$  kDa,  $\mathcal{D} = 1.07$ ) and  $P(\text{BLG}_{0.9}\text{-co-BLT}_{0.1})_{100}$  ( $M_n = 23.5$  kDa,  $\mathcal{D} = 1.07$ ).

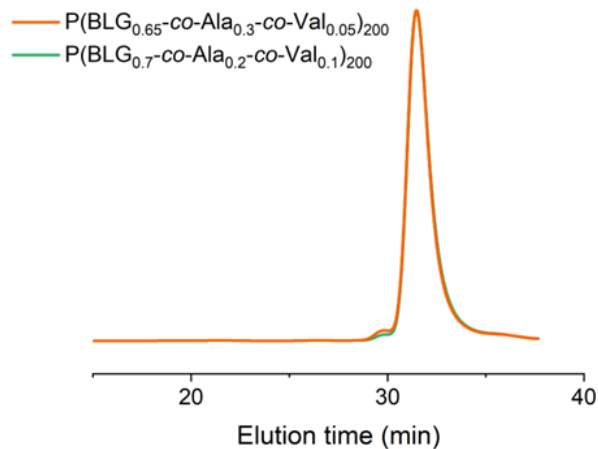


**Figure S8.** Characterization of BLG/Ala/Val-based copolypeptides synthesized from CE-catalyzed copolymerization initiated by PEG-PBLG. Normalized GPC-dRI trace of the resulting PEG-polypeptide with P(BLG<sub>0.65</sub>-co-Ala<sub>0.3</sub>-co-Val<sub>0.05</sub>)<sub>200</sub> ( $M_n = 37.8$  kDa,  $\mathcal{D} = 1.05$ ) and PEG-polypeptide with P(BLG<sub>0.7</sub>-co-Ala<sub>0.2</sub>-co-Val<sub>0.1</sub>)<sub>200</sub> ( $M_n = 40.4$  kDa,  $\mathcal{D} = 1.06$ ). The PEG segment was decomposed after deprotection by TMSI.

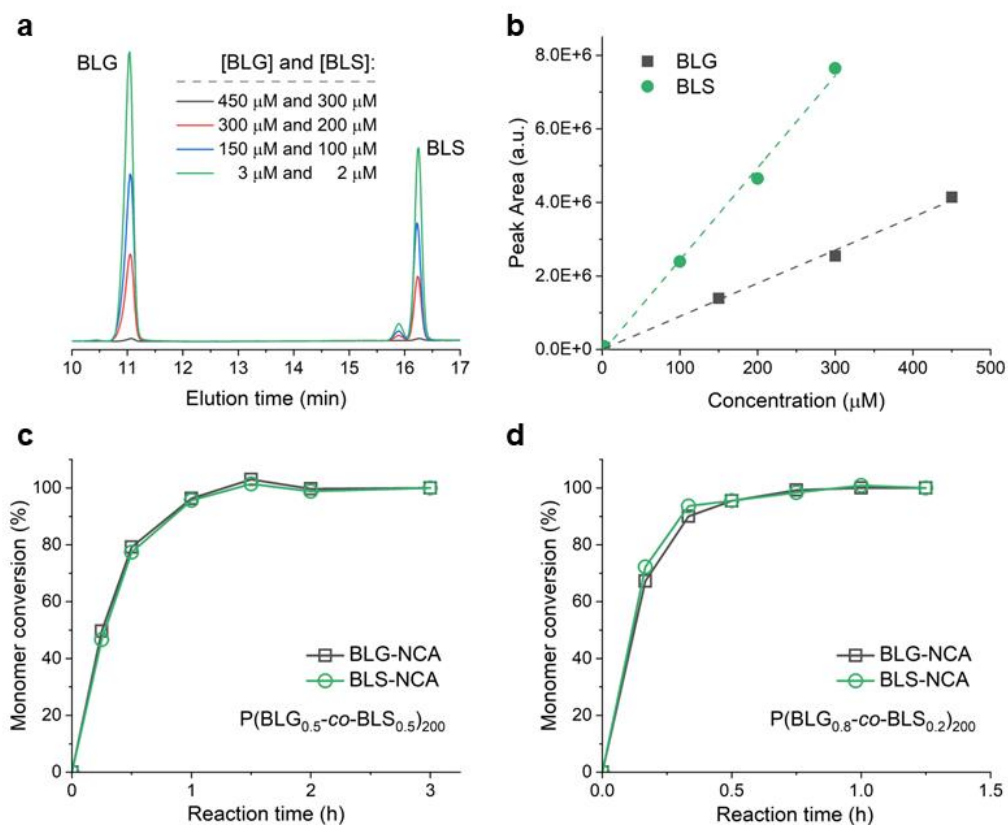


**Figure S9.** Determination of the randomness of  $\text{P}(\text{BLG}_{1-x}\text{-co-BLS}_x)_n$  copolypeptides prepared from SIMPLE copolymerization. (a) HPLC traces of the standard solutions of hydrolyzed BLG-NCA and BLS-NCA at various concentrations. (b) Validation of the linear relationship between absorbance at 202 nm and the concentrations of hydrolyzed BLG-NCA and BLS. The dash line is the linear regression fit. HPLC analysis for BLG and BLS concentrations at different polymerization time by detecting the signal for their products of hydrolysis. PEG-polypeptide with (c)  $\text{P}(\text{BLG}_{0.8}\text{-co-BLS}_{0.2})_{200}$  and (d) with  $\text{P}(\text{BLG}_{0.5}\text{-co-BLS}_{0.5})_{200}$ . The copolymerization kinetic profiles suggested high randomness of BLG and BLS residues distributed on the copolypeptide backbones, as the monomers consumed at similar rates during the copolymerization.

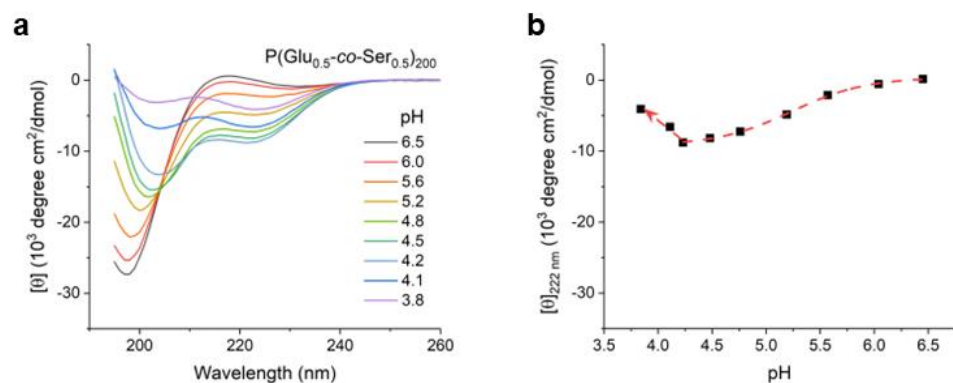


**Figure S10.** pH-induced conformational changes in P(Glu<sub>0.5</sub>-co-Ser<sub>0.5</sub>)<sub>200</sub>. (a) Conformational changes in P(Glu<sub>0.5</sub>-co-Ser<sub>0.5</sub>)<sub>200</sub> at different pHs at 25 °C, as monitored by CD spectroscopy. (b) Conformational transition at different pHs at 25 °C, as indicated by the molar ellipticity measured at 222 nm. The concentration of polypeptide was 0.1 mg/mL in a 15 mM acetate buffer, and the cuvette pathlength was 3 mm. The sample pH was tuned by 1 M NaOH and 1 M HCl solution. Data points in (b) were fit with a sigmoidal function (dashed line) to provide a visual guide.

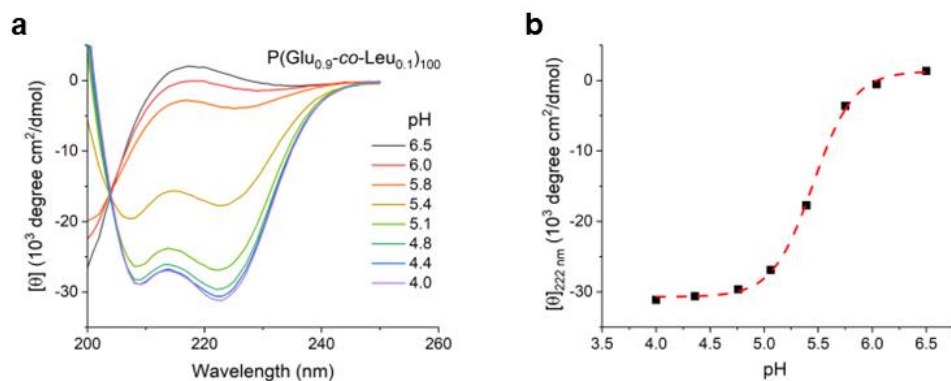


**Figure S11.** pH-induced conformational changes in P(Glu<sub>0.9</sub>-co-Leu<sub>0.1</sub>)<sub>100</sub>. (a) Conformational changes in P(Glu<sub>0.9</sub>-co-Leu<sub>0.1</sub>)<sub>100</sub> at different pHs at 25 °C, as monitored by CD spectroscopy. (b) Coil to helix transition at different pHs at 25 °C, as indicated by the molar ellipticity measured at 222 nm. The concentration of polypeptide was 0.1 mg/mL in a 15 mM acetate buffer, and the cuvette pathlength was 3 mm. The sample pH was tuned by 1 M NaOH and 1 M HCl solution. Data points in (b) were fit with a sigmoidal function (dashed line) to provide a visual guide.

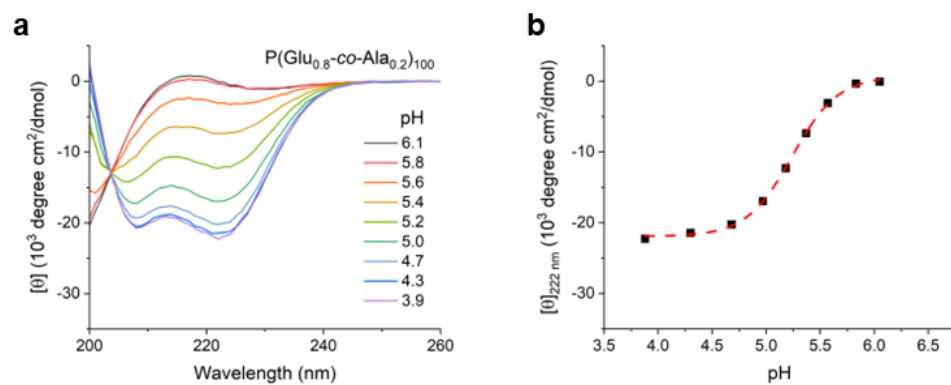


**Figure S12.** pH-induced conformational changes in P(Glu<sub>0.8</sub>-co-Ala<sub>0.2</sub>)<sub>100</sub>. (a) Conformational changes in P(Glu<sub>0.8</sub>-co-Ala<sub>0.2</sub>)<sub>100</sub> at different pHs at 25 °C, as monitored by CD spectroscopy. (b) Coil to helix transition at different pHs at 25 °C, as indicated by the molar ellipticity measured at 222 nm. The concentration of polypeptide was 0.1 mg/mL in a 15 mM acetate buffer, and the cuvette pathlength was 3 mm. The sample pH was tuned by 1 M NaOH and 1 M HCl solution. Data points in (b) were fit with a sigmoidal function (dashed line) to provide a visual guide.

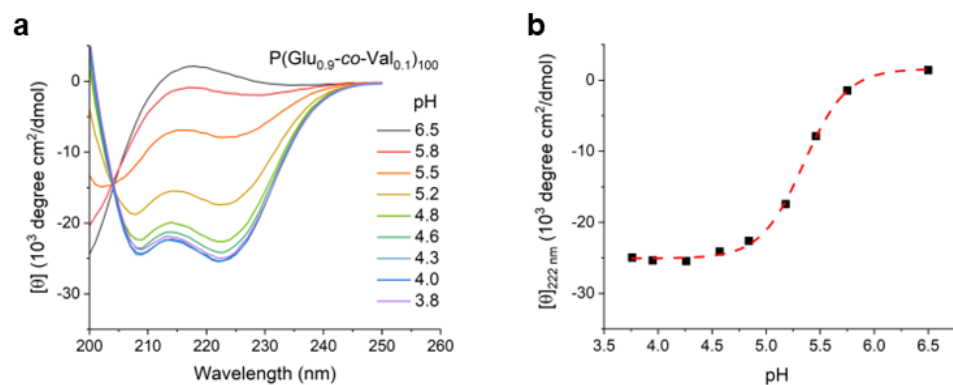


**Figure S13.** pH-induced conformational changes in P(Glu<sub>0.9</sub>-co-Val<sub>0.1</sub>)<sub>100</sub>. (a) Conformational changes in P(Glu<sub>0.9</sub>-co-Val<sub>0.1</sub>)<sub>100</sub> at different pHs at 25 °C, as monitored by CD spectroscopy. (b) Coil to helix transition at different pHs at 25 °C, as indicated by the molar ellipticity measured at 222 nm. The concentration of polypeptide was 0.1 mg/mL in a 15 mM acetate buffer, and the cuvette pathlength was 3 mm. The sample pH was tuned by 1 M NaOH and 1 M HCl solution. Data points in (b) were fit with a sigmoidal function (dashed line) to provide a visual guide.

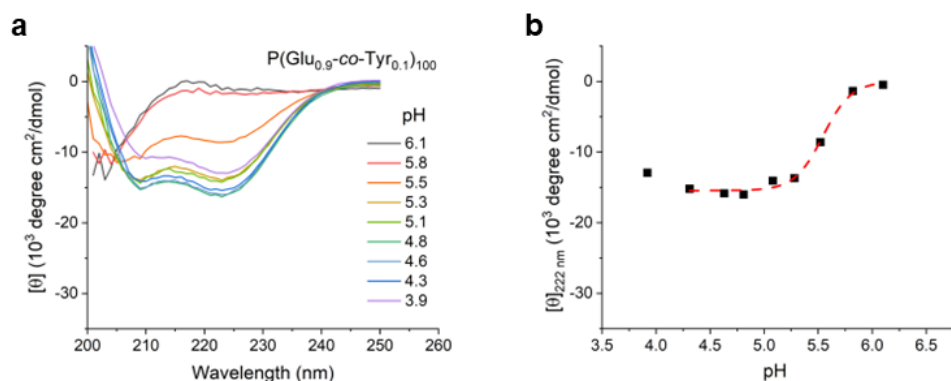


**Figure S14.** pH-induced conformational changes in P(Glu<sub>0.9</sub>-co-Tyr<sub>0.1</sub>)<sub>100</sub>. (a) Conformational changes in P(Glu<sub>0.9</sub>-co-Tyr<sub>0.1</sub>)<sub>100</sub> at different pHs at 25 °C, as monitored by CD spectroscopy. (b) Coil to helix transition at different pHs at 25 °C, as indicated by the molar ellipticity measured at 222 nm. The concentration of polypeptide was 0.1 mg/mL in a 15 mM acetate buffer, and the cuvette pathlength was 3 mm. The sample pH was tuned by 1 M NaOH and 1 M HCl solution. Data points in (b) were fit with a sigmoidal function (dashed line) to provide a visual guide.

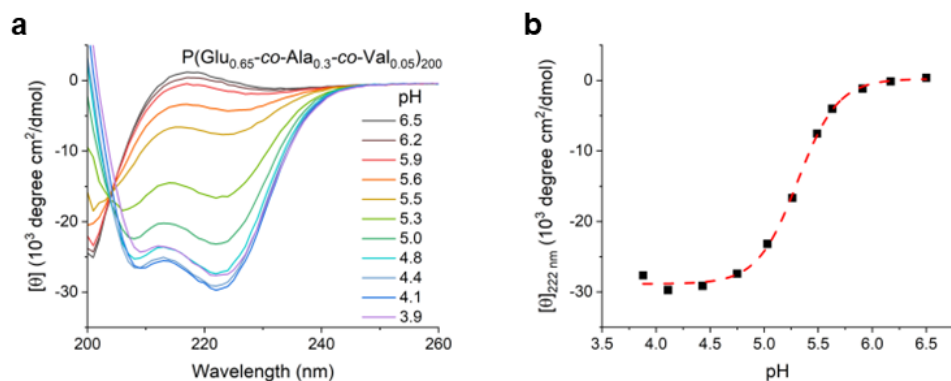


**Figure S15.** pH-induced conformational changes in  $P(\text{BLG}_{0.65}\text{-co-Ala}_{0.3}\text{-co-Val}_{0.05})_{200}$ . (a) Conformational changes in  $P(\text{BLG}_{0.65}\text{-co-Ala}_{0.3}\text{-co-Val}_{0.05})_{200}$  at different pHs at 25 °C, as monitored by CD spectroscopy. (b) Coil to helix transition at different pHs at 25 °C, as indicated by the molar ellipticity measured at 222 nm. The concentration of polypeptide was 0.1 mg/mL in a 15 mM acetate buffer, and the cuvette pathlength was 3 mm. The sample pH was tuned by 1 M NaOH and 1 M HCl solution. Data points in (b) were fit with a sigmoidal function (dashed line) to provide a visual guide.

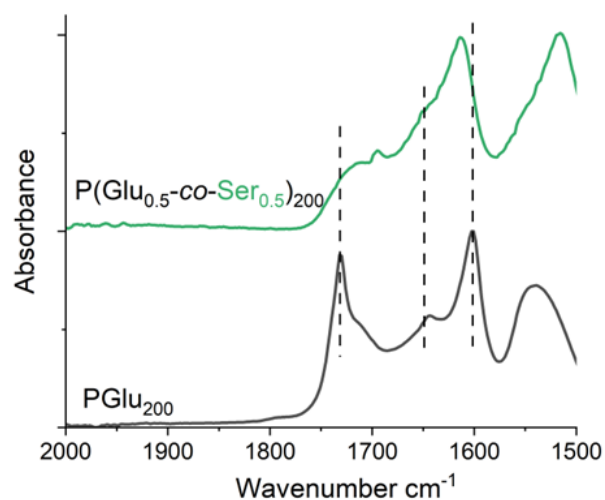


**Figure S16.** Conformational studies of the P(Glu)<sub>200</sub> and P(Glu<sub>0.5</sub>-co-Ser<sub>0.5</sub>)<sub>200</sub> supramolecular assemblies. Samples were lyophilized before FTIR-ATR measurements. For P(Glu) amyloid-like fibers, the peaks at 1730 and 1715 cm<sup>-1</sup> correspond to the stretching vibrations of the side chain carbonyl groups in  $\beta$ -sheet conformations, the peak at 1600 cm<sup>-1</sup> corresponds to the backbone carbonyl vibration (amide I) of  $\beta$ -sheets.<sup>14</sup> The peak at around 1645 cm<sup>-1</sup> corresponds to the backbone carbonyl vibration (amide I) of random coil conformation.<sup>16</sup> For P(Glu<sub>0.5</sub>-co-Ser<sub>0.5</sub>)<sub>200</sub>, the peaks at 1615 and 1695 cm<sup>-1</sup> correspond to the backbone carbonyl vibration (amide I) of  $\beta$ -sheet conformation of the serine residues.<sup>17</sup>

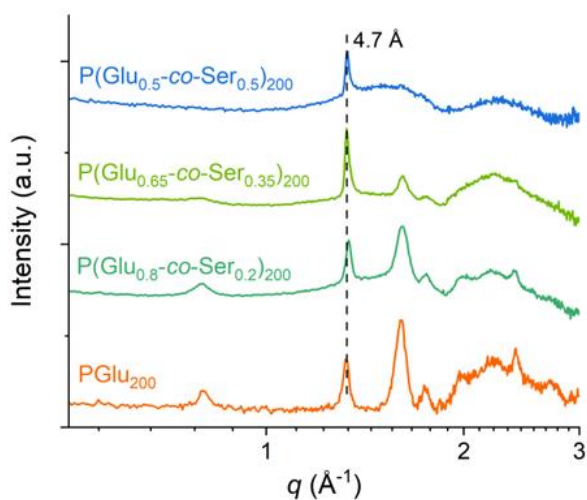


**Figure S17.** WAXS profiles of the supramolecular hydrogels of  $P(\text{Glu}_{1-x}\text{-co-Ser}_x)_n$ . The diffraction peak with a d-spacing of 4.7 Å corresponds to the hydrogen-bonded polypeptide main chain spacing under  $\beta$ -sheet conformation. The peak with a d-spacing of 3.9 Å was also encountered commonly in the cross- $\beta$  structure of P $\beta$ glu amyloid fibrils. The peak with a d-spacing of 7.9 Å corresponds to the packing distance between two juxtaposed P $\beta$ glu  $\beta$ -sheets, which sensitively depends on the local environment of polypeptide side chains.<sup>18</sup> The concentrations of polypeptide assemblies were 20 mg/mL.

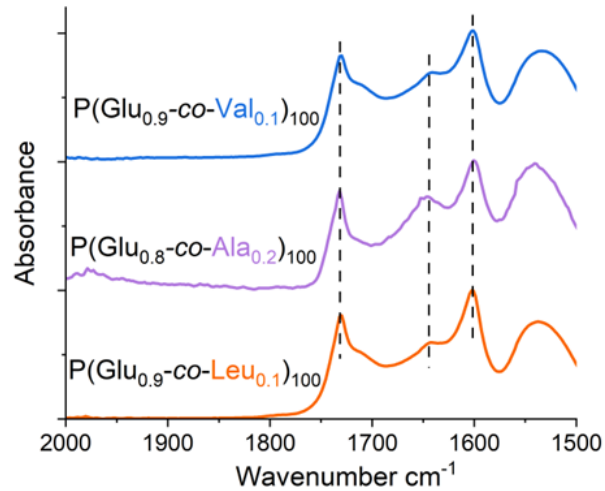


**Figure S18.** Conformational studies of the P(Glu<sub>0.9</sub>-co-Leu<sub>0.1</sub>)<sub>100</sub>, P(Glu<sub>0.8</sub>-co-Ala<sub>0.2</sub>)<sub>100</sub>, and P(Glu<sub>0.9</sub>-co-Val<sub>0.1</sub>)<sub>100</sub> supramolecular assemblies. Samples were lyophilized before FTIR-ATR measurements. The peak at around 1645 cm<sup>-1</sup> corresponds to the backbone carbonyl vibration (amide I) of random coil conformation.<sup>16</sup>

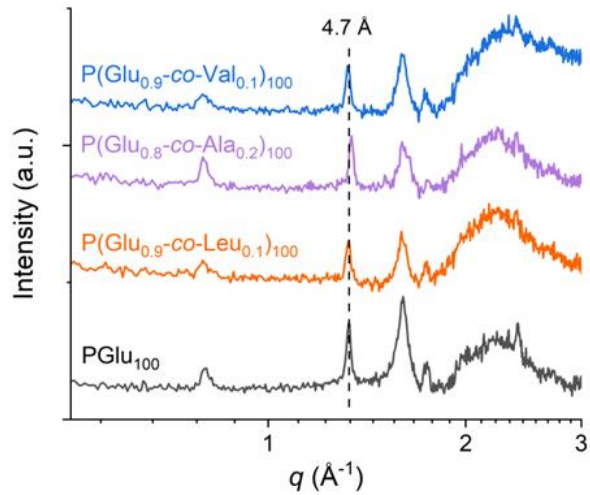


**Figure S19.** WAXS profiles of the supramolecular assemblies of bicomponent copolypeptides with nonpolar secondary amino acids. The diffraction peak with a d-spacing of 4.7 Å corresponds to the hydrogen-bonded polypeptide backbone separation with  $\beta$ -sheet conformation. The concentrations of polypeptide assemblies were 20 mg/mL.

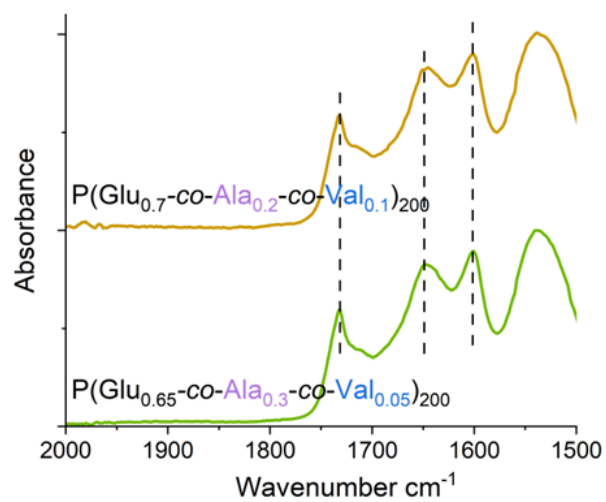


**Figure S20.** Conformational studies of the P(Glu<sub>1-x-y</sub>-co-Ala<sub>x</sub>-co-Val<sub>y</sub>)<sub>n</sub> supramolecular assemblies. Samples were lyophilized before FTIR-ATR measurements.

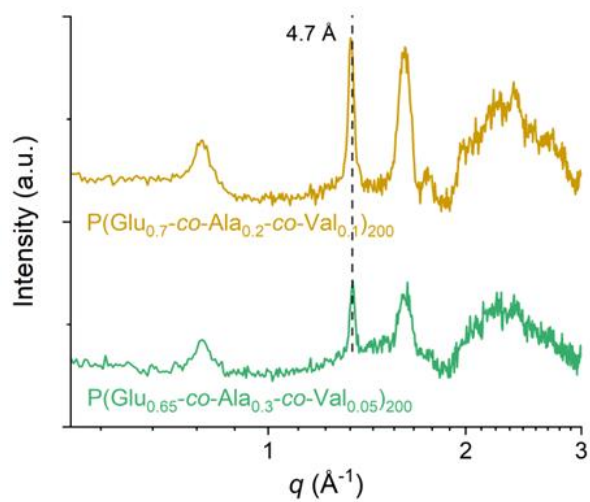


**Figure S21.** WAXS profiles of the  $P(\text{Glu}_{1-x-y}\text{-co-Ala}_x\text{-co-Val}_y)_n$  supramolecular hydrogels. The diffraction peak with a d-spacing of  $4.7 \text{ \AA}$  corresponds to the hydrogen-bonded polypeptide backbone separation with  $\beta$ -sheet conformation. The concentrations of polypeptide assemblies were  $20 \text{ mg/mL}$ .

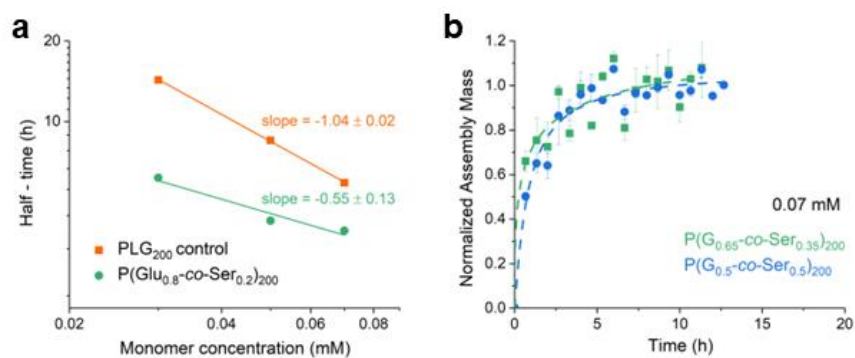


**Figure S22.** Supramolecular assembly kinetics of the  $P(\text{Glu}_{1-x}\text{-co-Ser}_x)_n$  copolypeptides in water. (a) Power-law scaling of the time to half-completion ( $t_{1/2}$ ) as a function of the initial monomer concentration during the assembly of  $\text{PGLu}_{200}$  and  $\text{P}(\text{Glu}_{0.8}\text{-co-Ser}_{0.2})_{200}$ , respectively. Data points (represented by solid symbols) were subjected to linear regression analysis (depicted by solid lines) to determine the slope, which corresponds to the scaling exponent. (b) Assembly kinetics of  $\text{P}(\text{Glu}_{0.65}\text{-co-Ser}_{0.35})_{200}$  and  $\text{P}(\text{Glu}_{0.5}\text{-co-Ser}_{0.5})_{200}$  at an initial monomer concentration of 0.07 mM, respectively. Data are representative of three replicate experiments. The dashed lines were provided for visual guidance. Since the assembly processes of  $\text{P}(\text{Glu}_{0.65}\text{-co-Ser}_{0.35})_{200}$  and  $\text{P}(\text{Glu}_{0.5}\text{-co-Ser}_{0.5})_{200}$  were so fast, the normalization of experimental kinetic data was difficult.

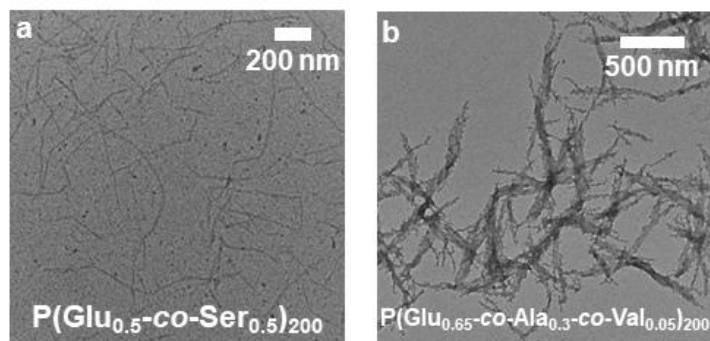


**Figure S23.** TEM images showcase the assembly of  $P(\text{Glu}_{0.5}\text{-co-Ser}_{0.5})_{200}$  into individual fibrils (a) and  $P(\text{Glu}_{0.65}\text{-co-Ala}_{0.3}\text{-co-Val}_{0.05})_{200}$  into fibril clusters (b), both in a 15 mM acetate buffer. These morphologies are similar to those shown in Figure 1d and in Figure 4c in the main text, which were prepared in water.

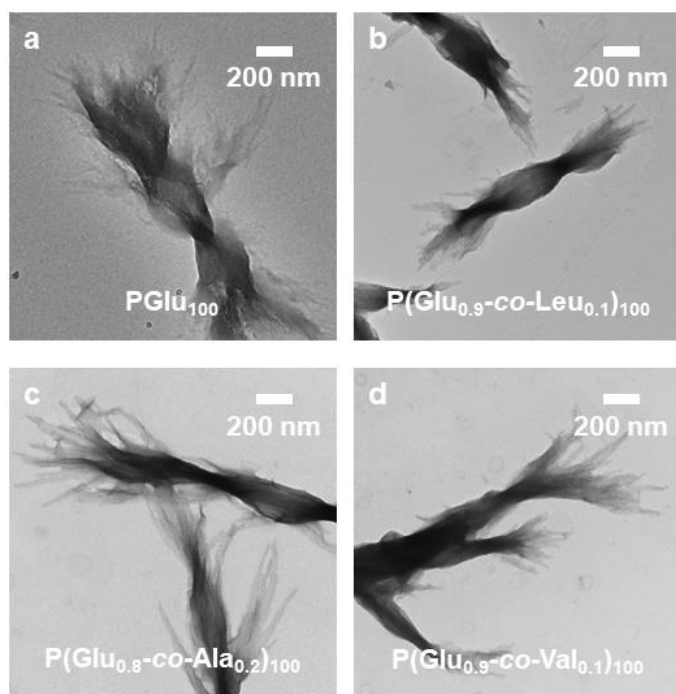


**Figure S24.** Negatively stained TEM of (a) P(Glu), (b) P(Glu<sub>0.9</sub>-co-Leu<sub>0.1</sub>)<sub>100</sub>, (c) P(Glu<sub>0.8</sub>-co-Ala<sub>0.2</sub>)<sub>100</sub>, and (d) P(Glu<sub>0.9</sub>-co-Val<sub>0.1</sub>)<sub>100</sub> amyloid fiber bundles. The individual protofibrils are around 10 nm wide.

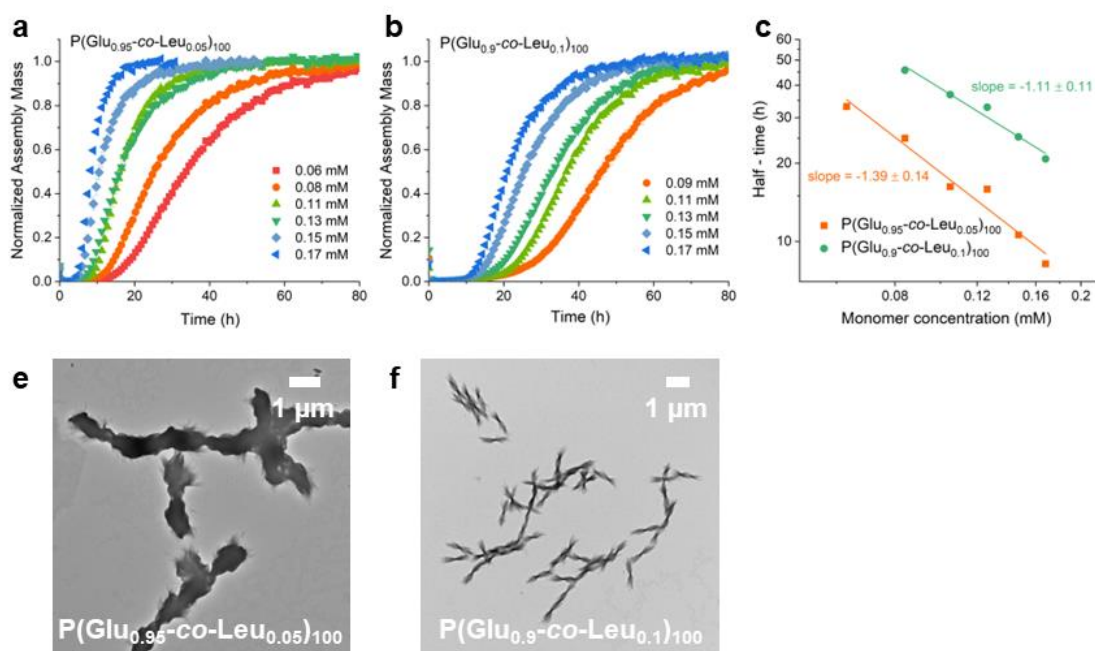


**Figure S25.** Supramolecular assembly of the  $P(\text{Glu}_{1-x}\text{-co-Leu}_x)_n$  copolypeptides in water. (a, b) Assembly kinetics of  $P(\text{Glu}_{0.95}\text{-co-Leu}_{0.05})_{100}$  and  $P(\text{Glu}_{0.9}\text{-co-Leu}_{0.1})_{100}$  at various initial monomer concentrations, respectively. Data are representative of three replicate experiments. (c) Power-law scaling of the time to half-completion ( $t_{1/2}$ ) as a function of the initial monomer concentration during the assembly of  $P(\text{Glu}_{0.95}\text{-co-Leu}_{0.05})_{100}$  and  $P(\text{Glu}_{0.9}\text{-co-Leu}_{0.1})_{100}$ , respectively. Data points (represented by solid symbols) were subjected to linear regression analysis (depicted by solid lines) to determine the slope, which corresponds to the scaling exponent. (e-f) TEM images of the assembled  $P(\text{Glu}_{0.95}\text{-co-Leu}_{0.05})_{100}$  and  $P(\text{Glu}_{0.9}\text{-co-Leu}_{0.1})_{100}$ , respectively.

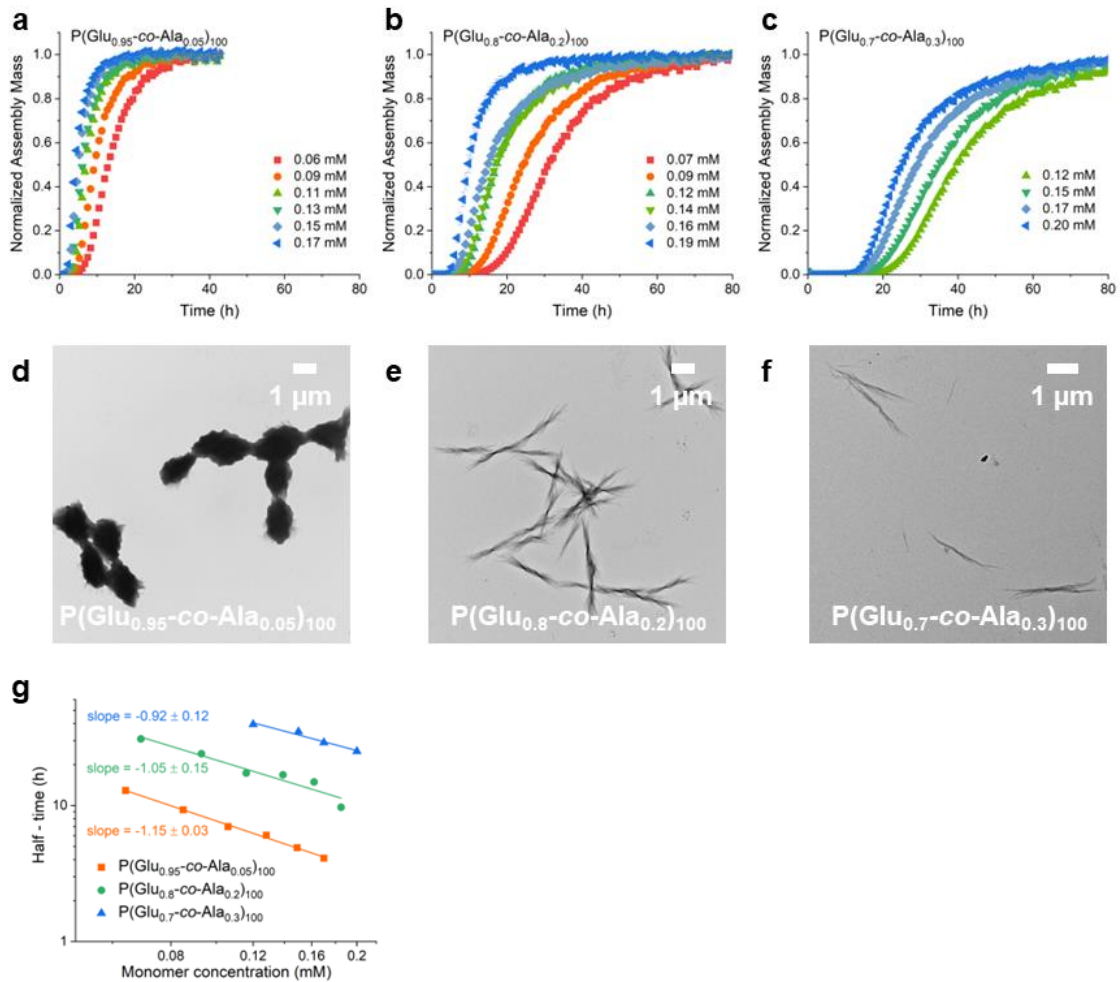


**Figure S26.** Supramolecular assembly of the  $P(\text{Glu}_{1-x}\text{-co-Ala}_x)_n$  copolypeptides in water. (a-c) Assembly kinetics of  $P(\text{Glu}_{0.95}\text{-co-Ala}_{0.05})_{100}$ ,  $P(\text{Glu}_{0.8}\text{-co-Ala}_{0.2})_{100}$ , and  $P(\text{Glu}_{0.7}\text{-co-Ala}_{0.3})_{100}$  at various initial monomer concentrations, respectively. Data are representative of three replicate experiments. (d-f) TEM images of the assembled  $P(\text{Glu}_{0.95}\text{-co-Ala}_{0.05})_{100}$ ,  $P(\text{Glu}_{0.8}\text{-co-Ala}_{0.2})_{100}$ , and  $P(\text{Glu}_{0.7}\text{-co-Ala}_{0.3})_{100}$ , respectively. (g) Power-law scaling of the time to half-completion ( $t_{1/2}$ ) as a function of the initial monomer concentration during the assembly of  $P(\text{Glu}_{0.95}\text{-co-Ala}_{0.05})_{100}$ ,  $P(\text{Glu}_{0.8}\text{-co-Ala}_{0.2})_{100}$ , and  $P(\text{Glu}_{0.7}\text{-co-Ala}_{0.3})_{100}$ , respectively. Data points (represented by solid symbols) were subjected to linear regression analysis (depicted by solid lines) to determine the slope, which corresponds to the scaling exponent.

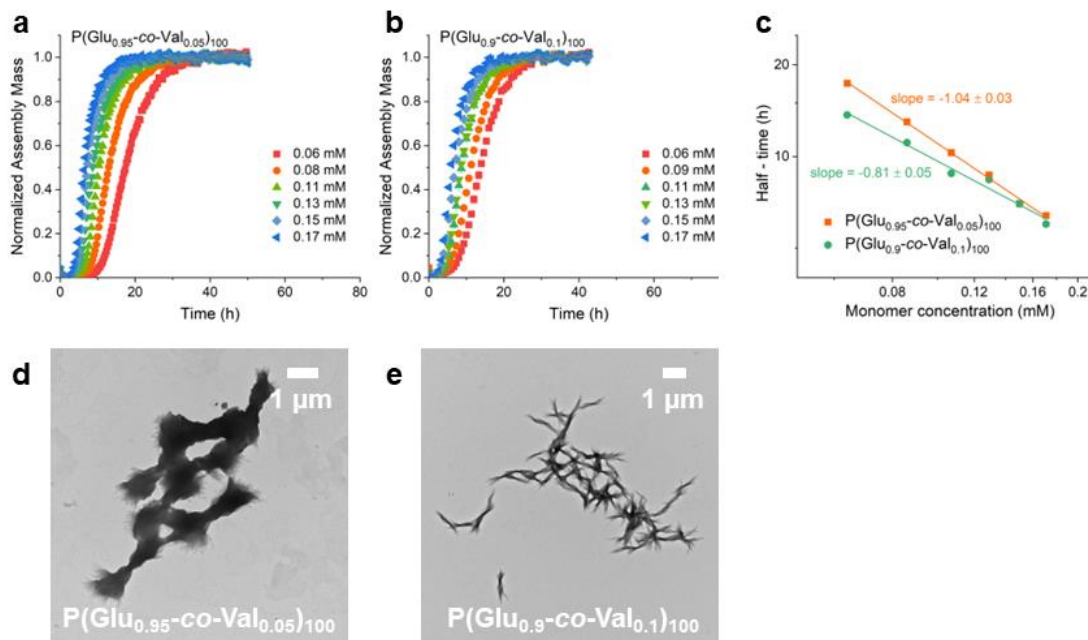


**Figure S27.** Supramolecular assembly of the P(Glu<sub>1-x</sub>-co-Val<sub>x</sub>)<sub>n</sub> copolypeptides in water. (a, b) Assembly kinetics of P(Glu<sub>0.95</sub>-co-Val<sub>0.05</sub>)<sub>100</sub> and P(Glu<sub>0.9</sub>-co-Val<sub>0.1</sub>)<sub>100</sub> at various initial monomer concentrations, respectively. Data are representative of three replicate experiments. (c) Power-law scaling of the time to half-completion ( $t_{1/2}$ ) as a function of the initial monomer concentration during the assembly of P(Glu<sub>0.95</sub>-co-Val<sub>0.05</sub>)<sub>100</sub> and P(Glu<sub>0.9</sub>-co-Val<sub>0.1</sub>)<sub>100</sub>, respectively. Data points (represented by solid symbols) were subjected to linear regression analysis (depicted by solid lines) to determine the slope, which corresponds to the scaling exponent. (d, e) TEM images of the assembled P(Glu<sub>0.95</sub>-co-Val<sub>0.05</sub>)<sub>100</sub> and P(Glu<sub>0.9</sub>-co-Val<sub>0.1</sub>)<sub>100</sub>, respectively.

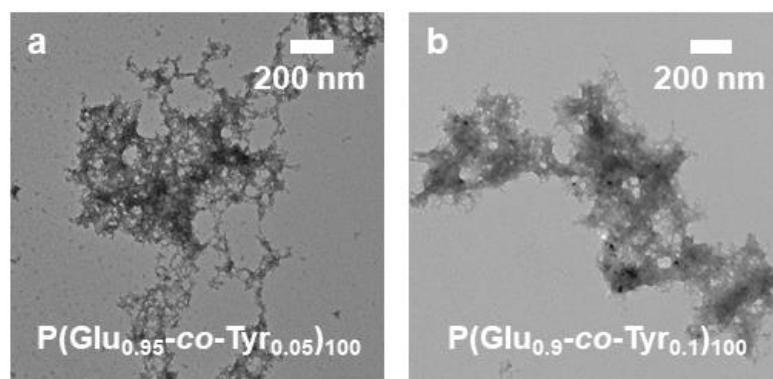


**Figure S28.** Amorphous aggregates from the  $P(\text{Glu}_{1-x}\text{-co-Tyr}_x)_n$  copolypeptides in water at pH 4.0. TEM images of the (a)  $P(\text{Glu}_{0.95}\text{-co-Tyr}_{0.05})_{100}$  and (b)  $P(\text{Glu}_{0.95}\text{-co-Tyr}_{0.05})_{100}$  aggregates.

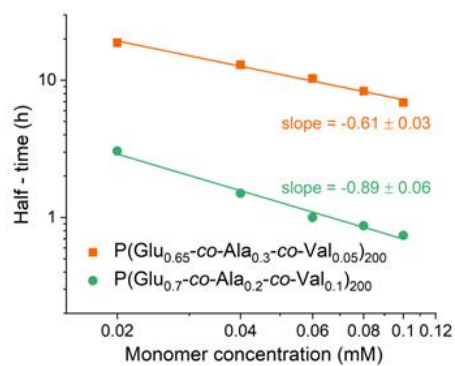


**Figure S29.** Power-law scaling of the time to half-completion ( $t_{1/2}$ ) as a function of the initial monomer concentration during the assembly of P(Glu<sub>0.65</sub>-co-Ala<sub>0.3</sub>-co-Val<sub>0.05</sub>)<sub>200</sub> and P(Glu<sub>0.7</sub>-co-Ala<sub>0.2</sub>-co-Val<sub>0.1</sub>)<sub>200</sub>, respectively. Data points (represented by solid symbols) were subjected to linear regression analysis (depicted by solid lines) to determine the slope, which corresponds to the scaling exponent.

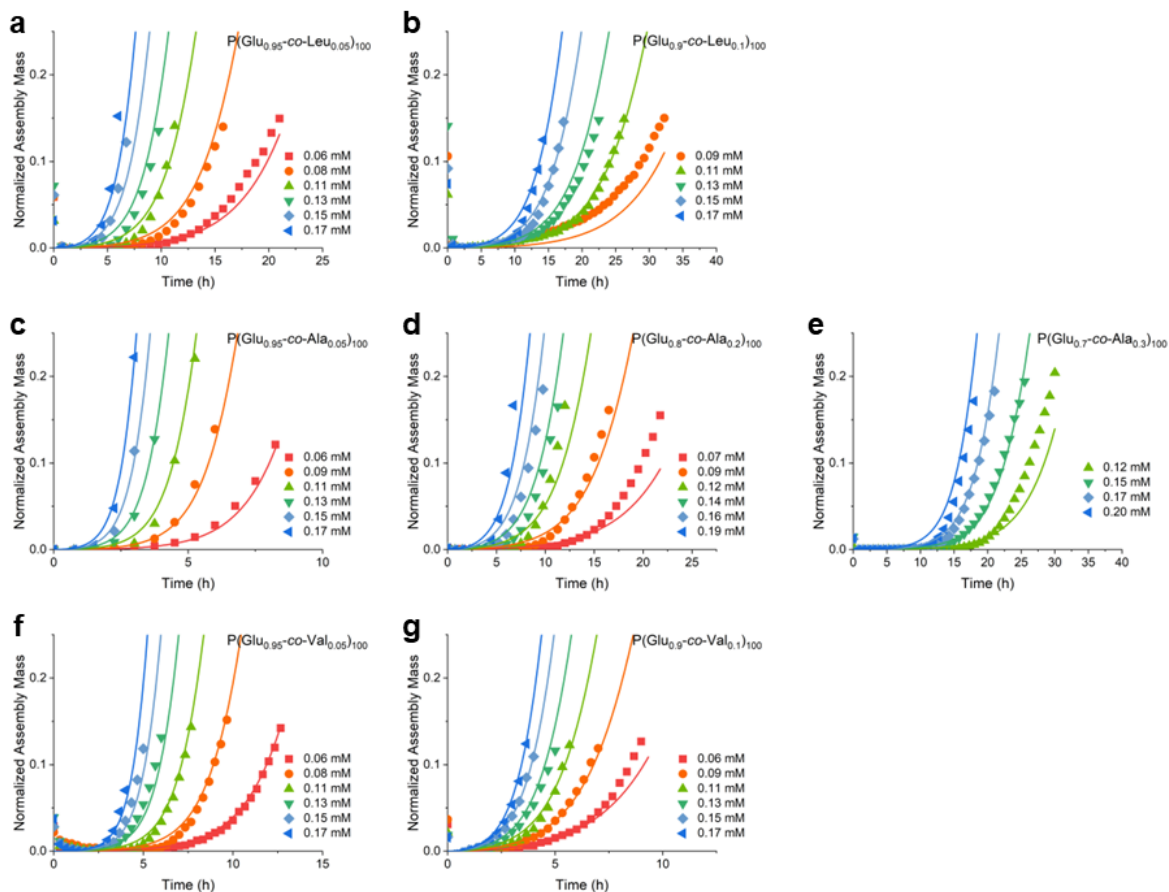


**Figure S30.** Early-stage global fit on the supramolecular assembly kinetics of (a)  $P(\text{Glu}_{0.95}\text{-co-Leu}_{0.05})_{100}$ , (b)  $P(\text{Glu}_{0.9}\text{-co-Leu}_{0.1})_{100}$ , (c)  $P(\text{Glu}_{0.95}\text{-co-Ala}_{0.05})_{100}$ , (d)  $P(\text{Glu}_{0.8}\text{-co-Ala}_{0.2})_{100}$ , (e)  $P(\text{Glu}_{0.7}\text{-co-Ala}_{0.3})_{100}$ , (f)  $P(\text{Glu}_{0.95}\text{-co-Val}_{0.05})_{100}$ , and (g)  $P(\text{Glu}_{0.9}\text{-co-Val}_{0.1})_{100}$  based on secondary nucleation model. From the optimized fitting, the critical nucleus sizes of primary nucleation ( $n_c$ ) and secondary nucleation ( $n_2$ ) were determined to be 3 and 1 for the  $P(\text{Glu}_{1-x}\text{-co-Leu}_x)_n$  assembly processes, 3 and 1 for the  $P(\text{Glu}_{1-x}\text{-co-Ala}_x)_n$  assembly processes, and 2 and 1 for the  $P(\text{Glu}_{1-x}\text{-co-Val}_x)_n$  assembly processes.

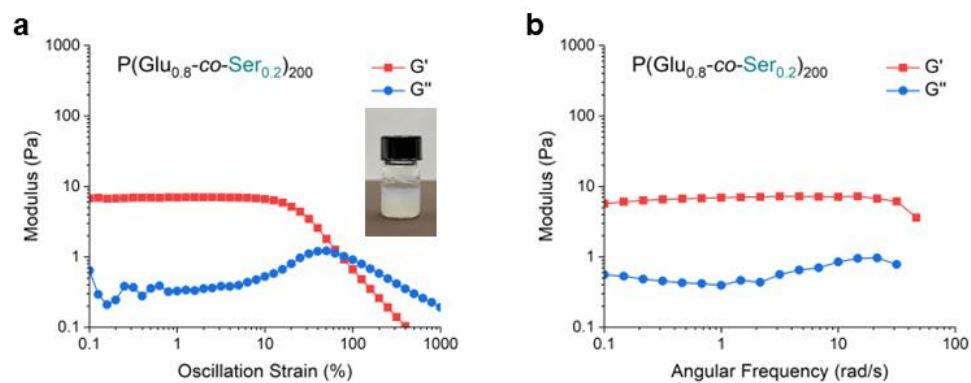


**Figure S31.** Rheological properties of the  $P(\text{Glu}_{0.8}\text{-co-Ser}_{0.2})_{200}$  viscous solution. (a) Left: Strain-dependent oscillatory rheology ( $\omega = 1.0$  rad/s, 25 °C). Right: photographs of its viscous solution at 20 mg/mL. (b) Frequency dependent oscillatory rheology (0.5% strain, 25 °C). The hydrogel concentration was 20 mg/mL.

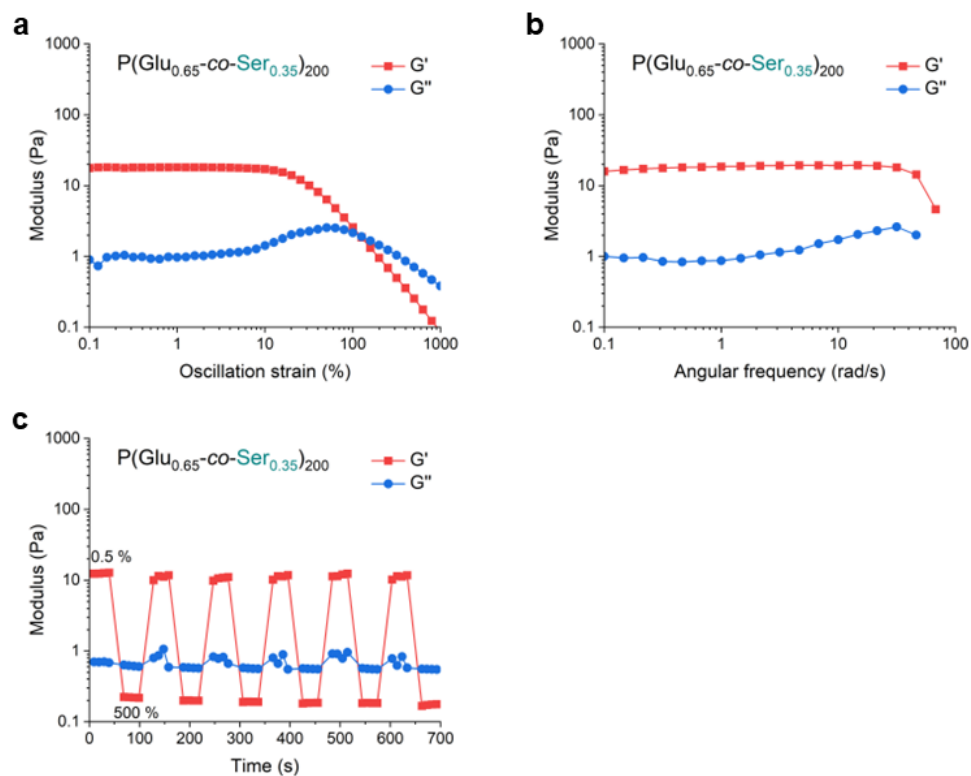


**Figure S32.** Rheological properties of the P(Glu<sub>0.65</sub>-co-Ser<sub>0.35</sub>)<sub>200</sub> supramolecular polymer hydrogel. (a) Strain-dependent oscillatory rheology ( $\omega = 1.0$  rad/s, 25 °C). (b) Frequency dependent oscillatory rheology (0.5% strain, 25 °C). (c) Oscillatory rheology alternating between 0.5 and 500% strain for the 30-s periods ( $\omega = 1.0$  rad/s, 25 °C) shows self-healing property. The hydrogel concentration was 20 mg/mL.

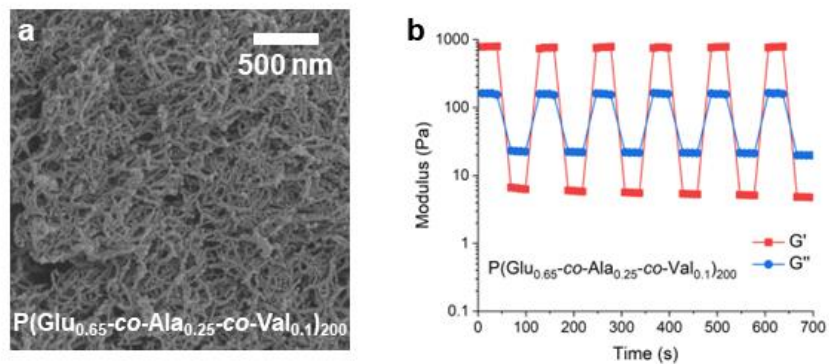


**Figure S33.** Fibril network and rheological properties of the  $P(\text{Glu}_{0.65}\text{-co-Ala}_{0.25}\text{-co-Val}_{0.1})_{200}$  supramolecular polymer hydrogel. (a) SEM image of  $P(\text{Glu}_{0.65}\text{-co-Ala}_{0.25}\text{-co-Val}_{0.1})_{200}$  hydrogel post supercritical  $\text{CO}_2$  drying. (b) Oscillatory rheology profile for the same hydrogel, cycling between 0.5% and 500% strain at a constant angular frequency ( $\omega = 1.0$  rad/s) and temperature (25 °C). The hydrogel concentration was 20 mg/mL.

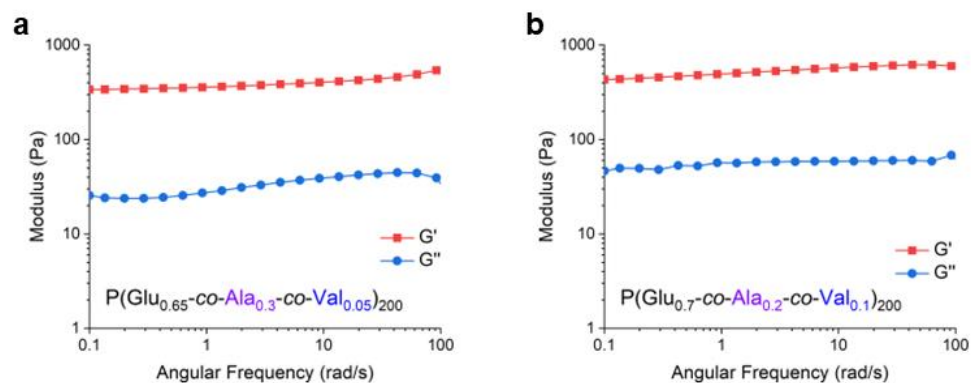


**Figure S34.** Frequency dependent oscillatory rheology (0.5% strain, 25 °C) of (a)  $P(\text{Glu}_{0.65}\text{-co-Ala}_{0.3}\text{-co-Val}_{0.05})_{200}$  and (b)  $P(\text{Glu}_{0.7}\text{-co-Ala}_{0.2}\text{-co-Val}_{0.1})_{200}$  supramolecular hydrogels. The hydrogel concentrations were 20 mg/mL.

#### 4. Supplementary Tables.

**Table S1.** Summary of the synthesis of PEG polypeptides containing random copolypeptides<sup>a</sup>

Entry	Composition	Expected ratio <sup>b</sup>	Obtained ratio in polymer <sup>c</sup>	[M] <sub>0</sub> /[I] <sub>0</sub> <sup>d</sup>	M <sub>n</sub> /M <sub>n</sub> <sup>*e,f</sup> (kDa)	D <sup>g</sup>
1	PBLG <sub>200</sub>	100:0	100:0	200	48.3/50.4	1.05
2	P(BLG <sub>0.8-co-BLS</sub> <sub>0.2</sub> ) <sub>200</sub>	80:20	79:21	200	46.3/48.8	1.05
3	P(BLG <sub>0.5-co-BLS</sub> <sub>0.5</sub> ) <sub>200</sub>	50:50	49:51	200	45.2/46.4	1.05
4	P(BLG <sub>0.95-co-Leu</sub> <sub>0.05</sub> ) <sub>100</sub>	95:5	95:5	100	19.2/21.4	1.05
5	P(BLG <sub>0.9-co-Leu</sub> <sub>0.1</sub> ) <sub>100</sub>	90:10	91:9	100	19.0/20.8	1.05
6	P(BLG <sub>0.85-co-Leu</sub> <sub>0.15</sub> ) <sub>100</sub>	85:15	84:16	100	19.3/20.3	1.05
7	P(BLG <sub>0.95-co-Ala</sub> <sub>0.05</sub> ) <sub>100</sub>	95:5	91:9	100	17.6/21.2	1.05
8	P(BLG <sub>0.8-co-Ala</sub> <sub>0.2</sub> ) <sub>100</sub>	80:20	77:23	100	18.1/18.9	1.08
9	P(BLG <sub>0.7-co-Ala</sub> <sub>0.3</sub> ) <sub>100</sub>	70:30	68:32	100	16.9/17.5	1.07
10	P(BLG <sub>0.95-co-Val</sub> <sub>0.05</sub> ) <sub>100</sub>	95:5	96:4	100	19.5/21.3	1.05
11	P(BLG <sub>0.9-co-Val</sub> <sub>0.1</sub> ) <sub>100</sub>	90:10	93:7	100	18.5/20.7	1.05
12	P(BLG <sub>0.85-co-Val</sub> <sub>0.15</sub> ) <sub>100</sub>	85:15	90:10	100	17.4/20.1	1.05
13	P(BLG <sub>0.65-co-Ala</sub> <sub>0.3-co-Val</sub> <sub>0.05</sub> ) <sub>200</sub>	65:30:5	61:32:7	200	37.8/40.3	1.05
14	P(BLG <sub>0.7-co-Ala</sub> <sub>0.2-co-Val</sub> <sub>0.1</sub> ) <sub>200</sub>	70:20:10	68:22:10	200	40.4/42.0	1.05

<sup>a</sup>The conversion of NCA intermediate was above 99% as confirmed by FTIR. Random copolypeptides were prepared from the polymerization of NCA mixture. <sup>b</sup>Expected composition. <sup>c</sup>Obtained composition in obtained polypeptides from <sup>1</sup>H NMR. <sup>d</sup>The designed monomer-to-initiator ([M]<sub>0</sub>/[I]<sub>0</sub>) ratio for polymerizations. <sup>e</sup>MWs obtained by GPC. <sup>f</sup>Obtained MWs/expected MWs\*. <sup>g</sup>Polydispersity index obtained by GPC.

**Table S2.** Rate constants obtained from the global analysis of copolypeptides assembly kinetics.

Entry	Composition	$n_c$	$n_2$	$k_n \times k_+$ ( $M^{-n_c} h^{-2}$ )	$k_2 \times k_+$ ( $M^{-n_2-1} h^{-2}$ )
1	P(BLG <sub>0.95-co-Leu</sub> <sub>0.05</sub> ) <sub>100</sub>	3	1	$1.61 \times 10^8$	$8.94 \times 10^6$
2	P(BLG <sub>0.9-co-Leu</sub> <sub>0.1</sub> ) <sub>100</sub>	3	1	$2.95 \times 10^7$	$1.79 \times 10^6$
3	P(BLG <sub>0.95-co-Ala</sub> <sub>0.05</sub> ) <sub>100</sub>	3	1	$5.44 \times 10^8$	$7.11 \times 10^7$
4	P(BLG <sub>0.8-co-Ala</sub> <sub>0.2</sub> ) <sub>100</sub>	3	1	$1.19 \times 10^8$	$5.36 \times 10^6$
5	P(BLG <sub>0.7-co-Ala</sub> <sub>0.3</sub> ) <sub>100</sub>	3	1	$4.23 \times 10^6$	$1.96 \times 10^6$
6	P(BLG <sub>0.95-co-Val</sub> <sub>0.05</sub> ) <sub>100</sub>	2	1	$1.47 \times 10^4$	$3.52 \times 10^7$
7	P(BLG <sub>0.9-co-Val</sub> <sub>0.1</sub> ) <sub>100</sub>	2	1	$1.02 \times 10^5$	$2.28 \times 10^7$

$n_c$ , nucleus size of the primary nucleation process.

$n_2$ , nucleus size of the secondary nucleation process.

$k_n$ , the rate constant for the formation of the primary nucleus.

$k_+$ , the fibril elongation rate constant.

$k_2$ , the secondary nucleus formation rate constant.

## 5. NMR spectra.

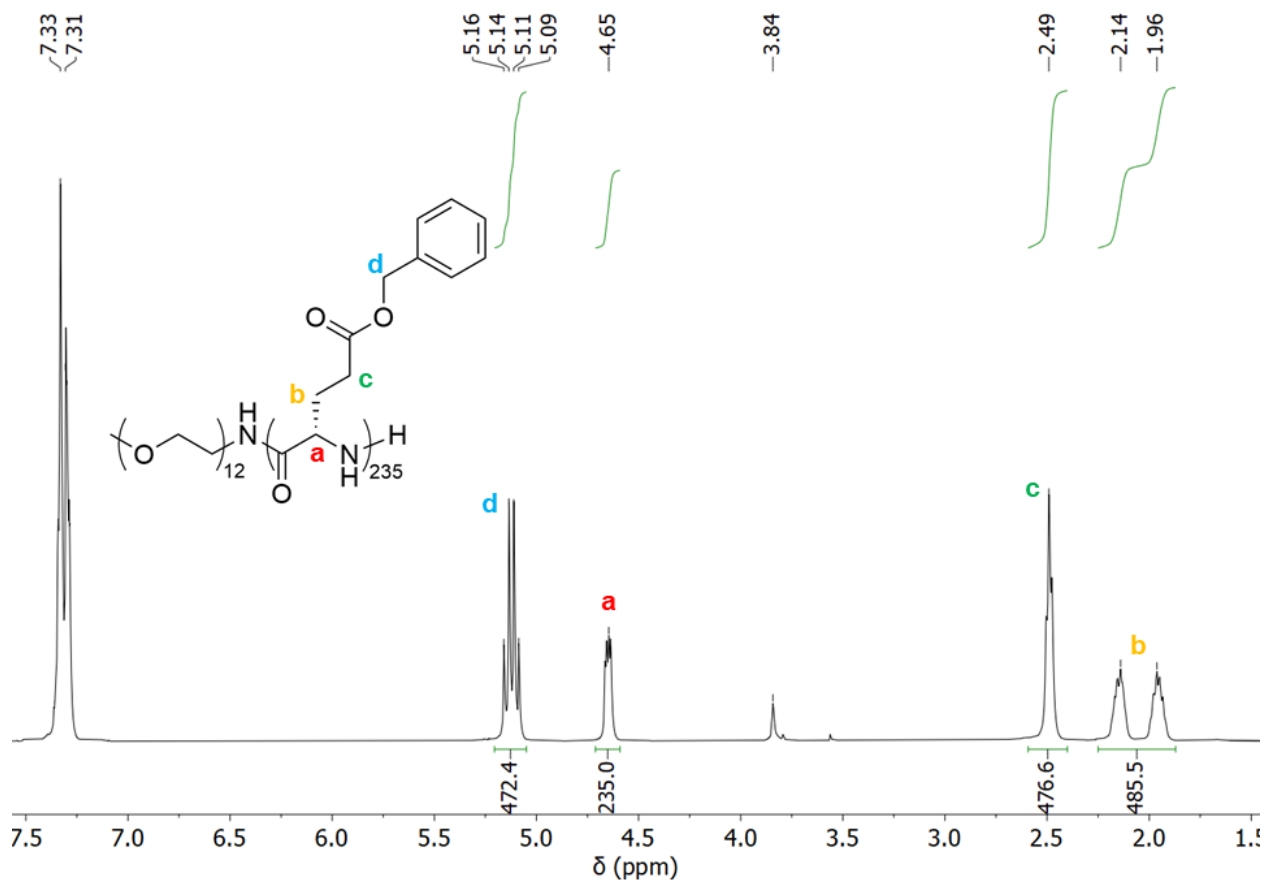


**Figure S35.**  $^1\text{H}$  NMR spectrum of PEG-polypeptide with PBLG<sub>200</sub> in  $\text{CDCl}_3/\text{TFA-}d$  (70:30, v/v).

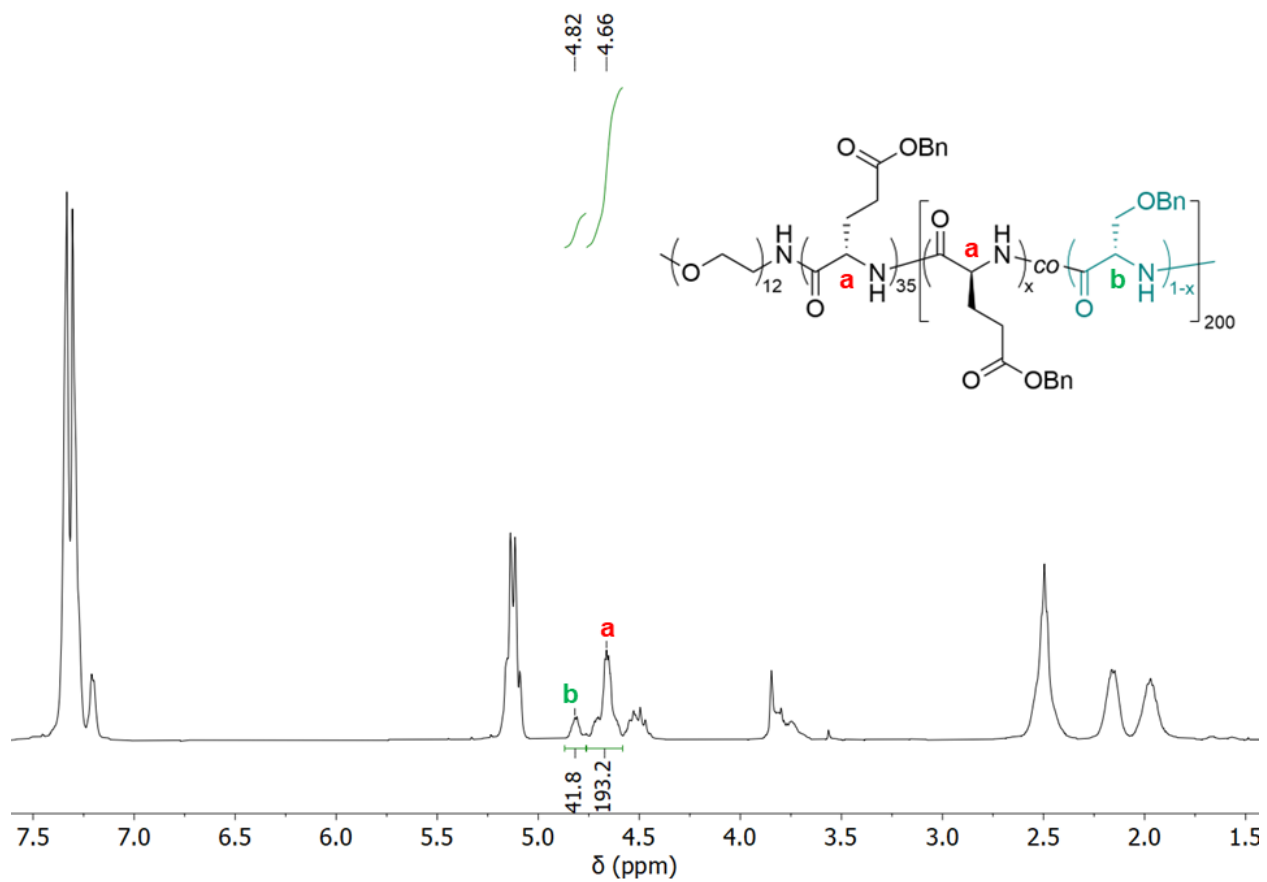


**Figure S36.**  $^1\text{H}$  NMR spectrum of PEG-polypeptide with  $\text{P}(\text{BLG}_{0.8}\text{-co-BLS}_{0.2})_{200}$  in  $\text{CDCl}_3/\text{TFA-}d$  (70:30, v/v).

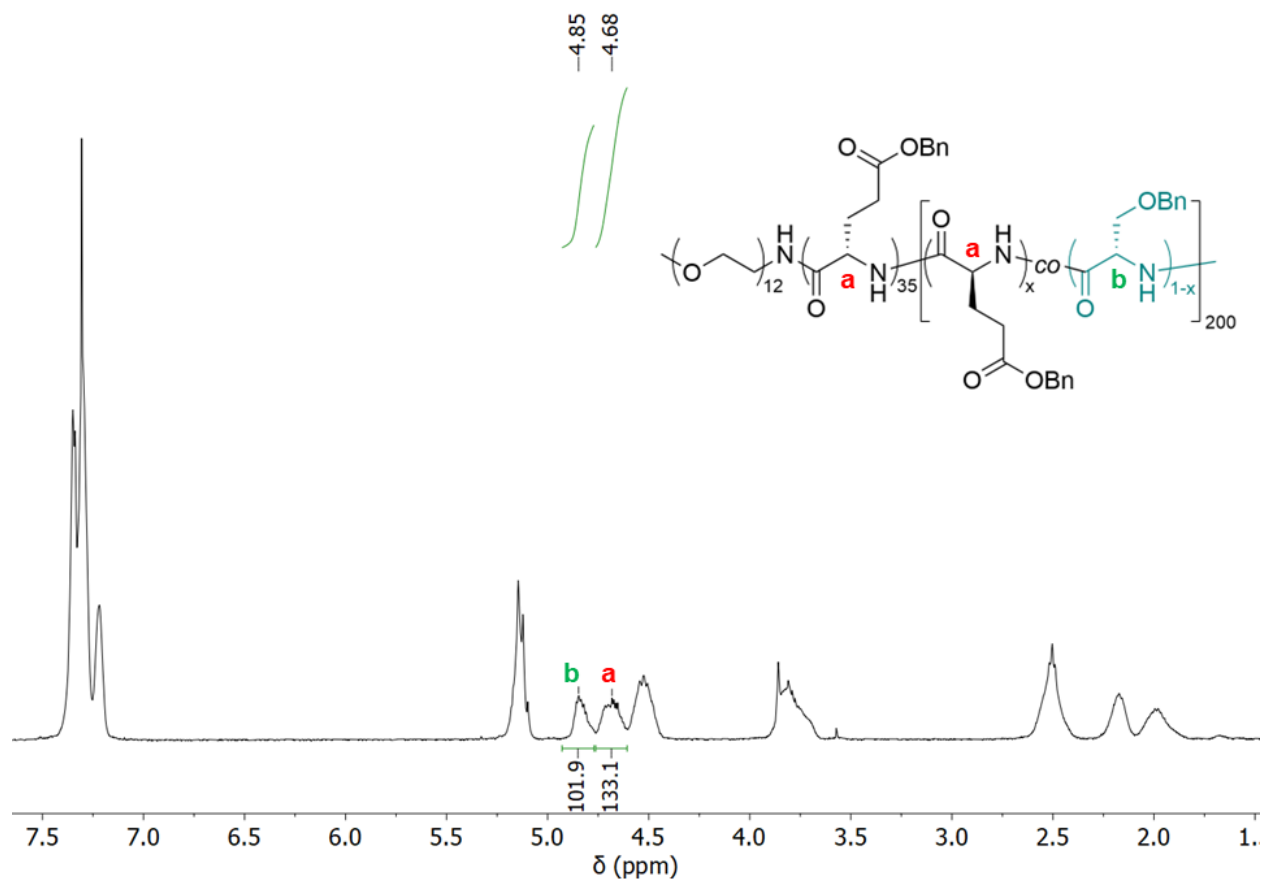


**Figure S37.**  $^1\text{H}$  NMR spectrum of PEG-polypeptide with  $\text{P}(\text{BLG}_{0.5}\text{-co-BLS}_{0.5})_{200}$  in  $\text{CDCl}_3/\text{TFA-}d$  (70:30, v/v).

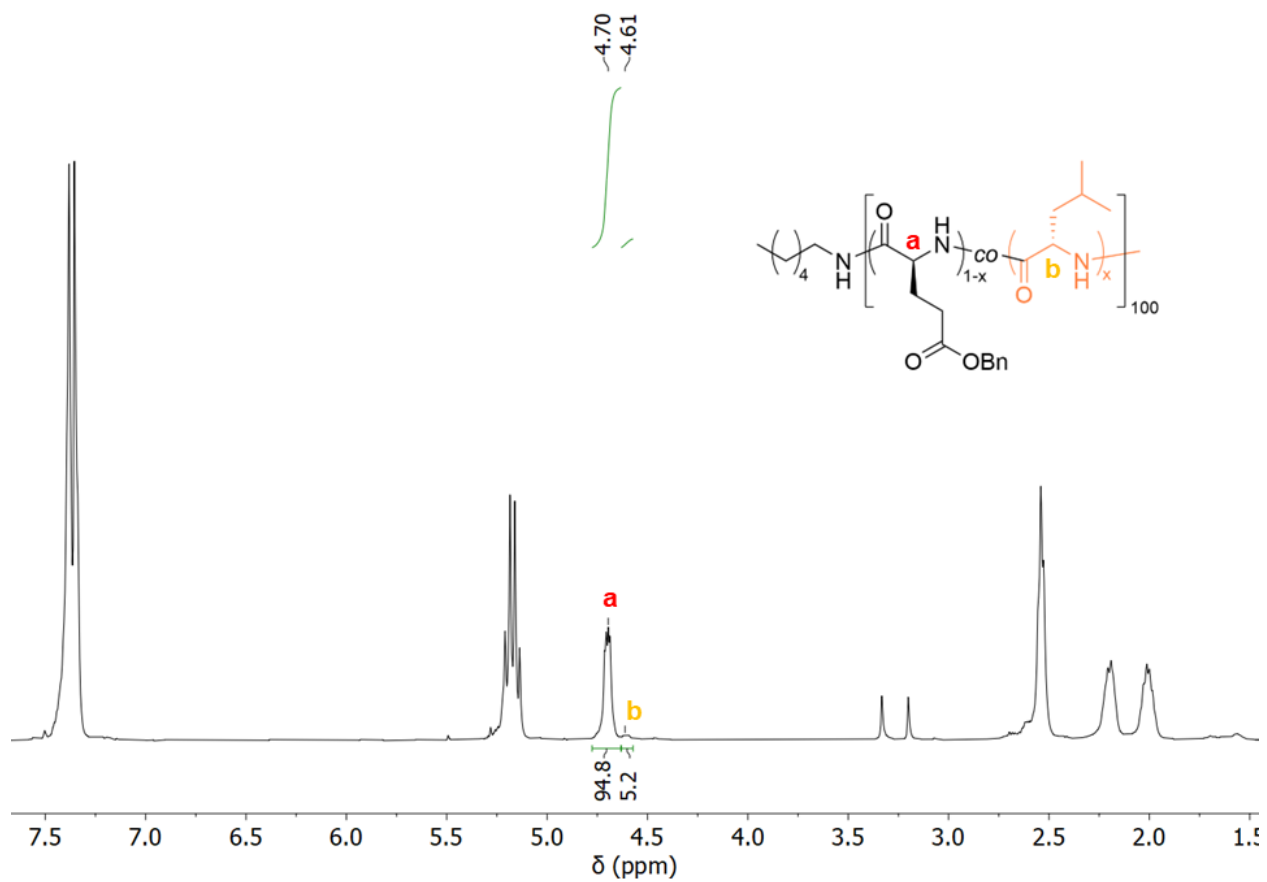


**Figure S38.**  $^1\text{H}$  NMR spectrum of  $\text{P}(\text{BLG}_{0.95}\text{-co-Leu}_{0.05})_{100}$  in  $\text{CDCl}_3/\text{TFA-}d$  (70:30, v/v).

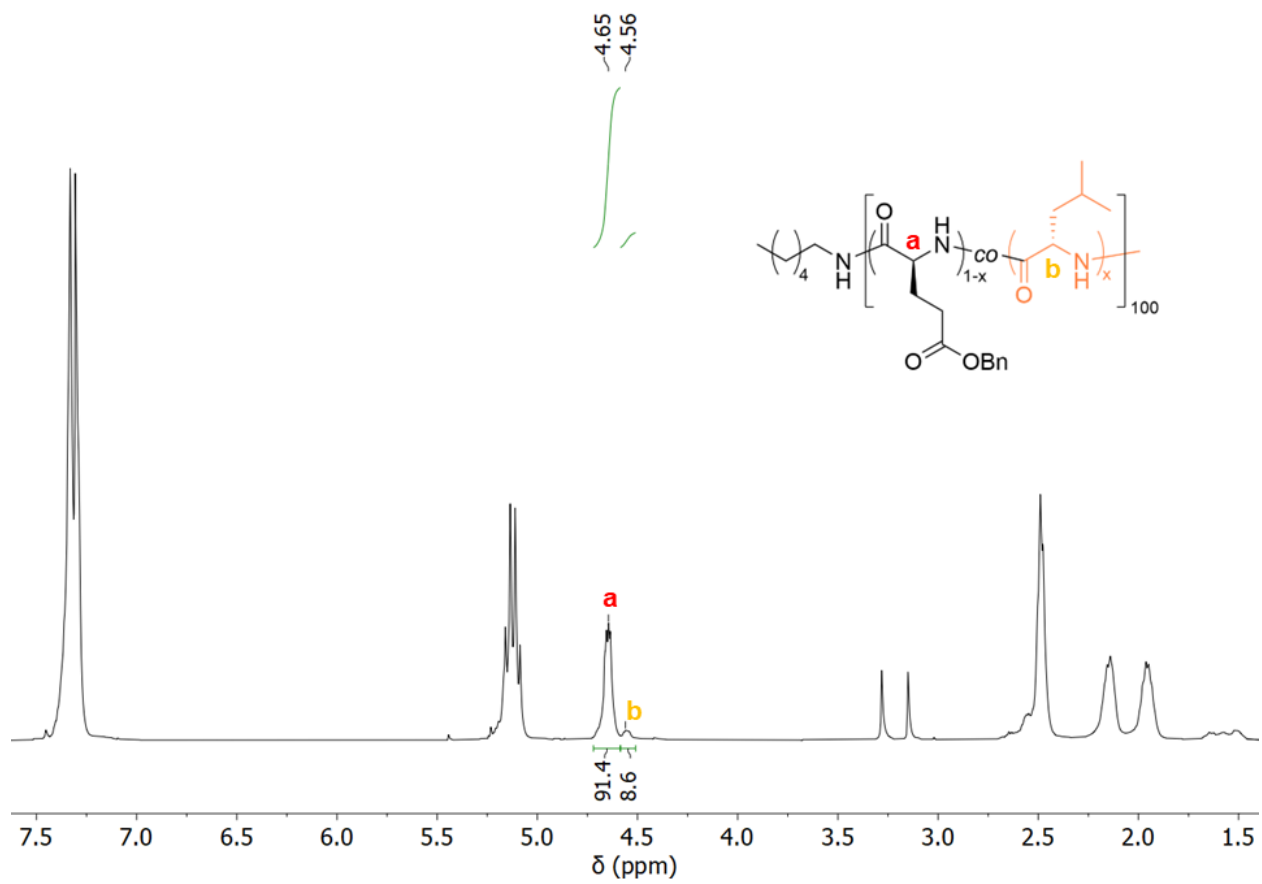


**Figure S39.**  $^1\text{H}$  NMR spectrum of  $\text{P}(\text{BLG}_{0.9}\text{-co-Leu}_{0.1})_{100}$  in  $\text{CDCl}_3/\text{TFA-}d$  (70:30, v/v).

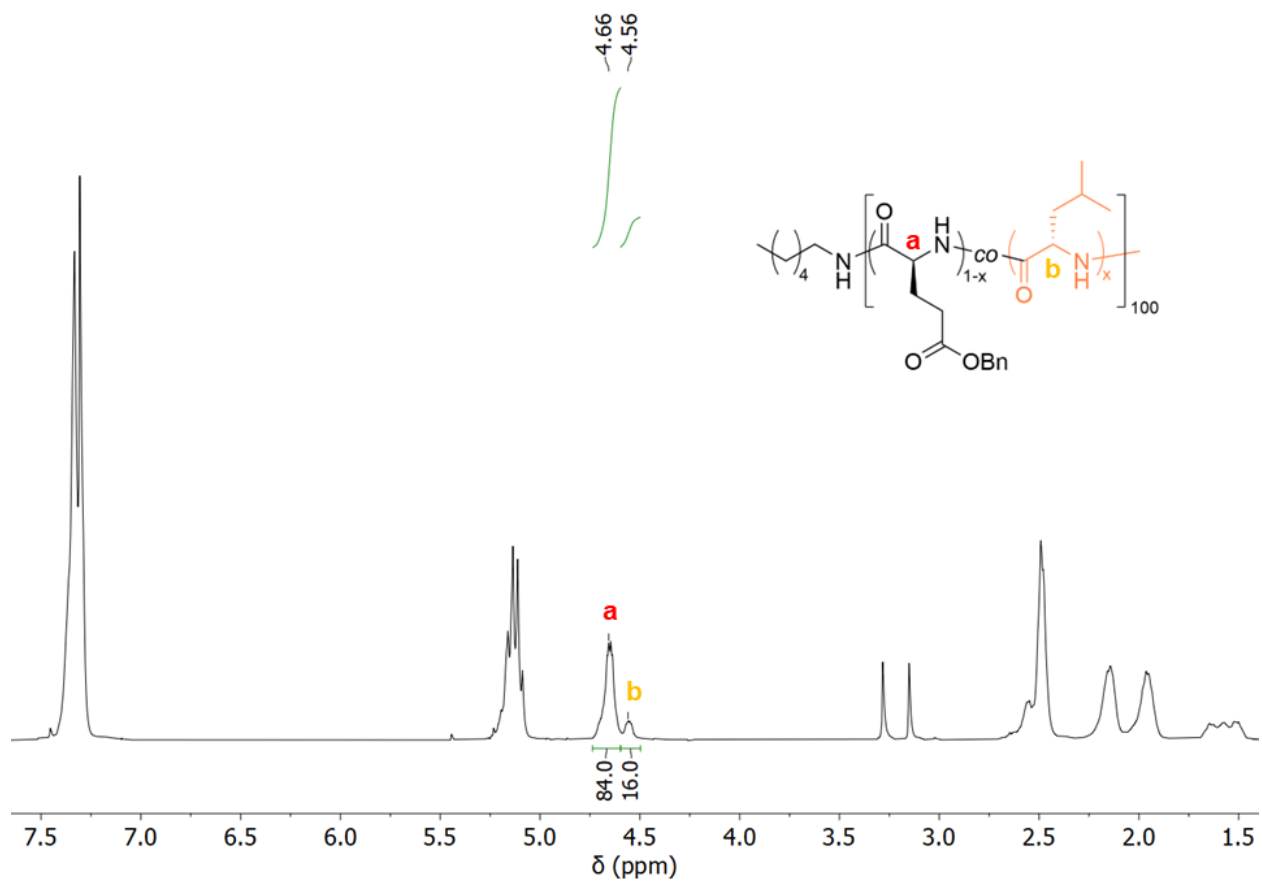


**Figure S40.**  $^1\text{H}$  NMR spectrum of  $\text{P}(\text{BLG}_{0.85}\text{-co-Leu}_{0.15})_{100}$  in  $\text{CDCl}_3/\text{TFA-}d$  (70:30, v/v).

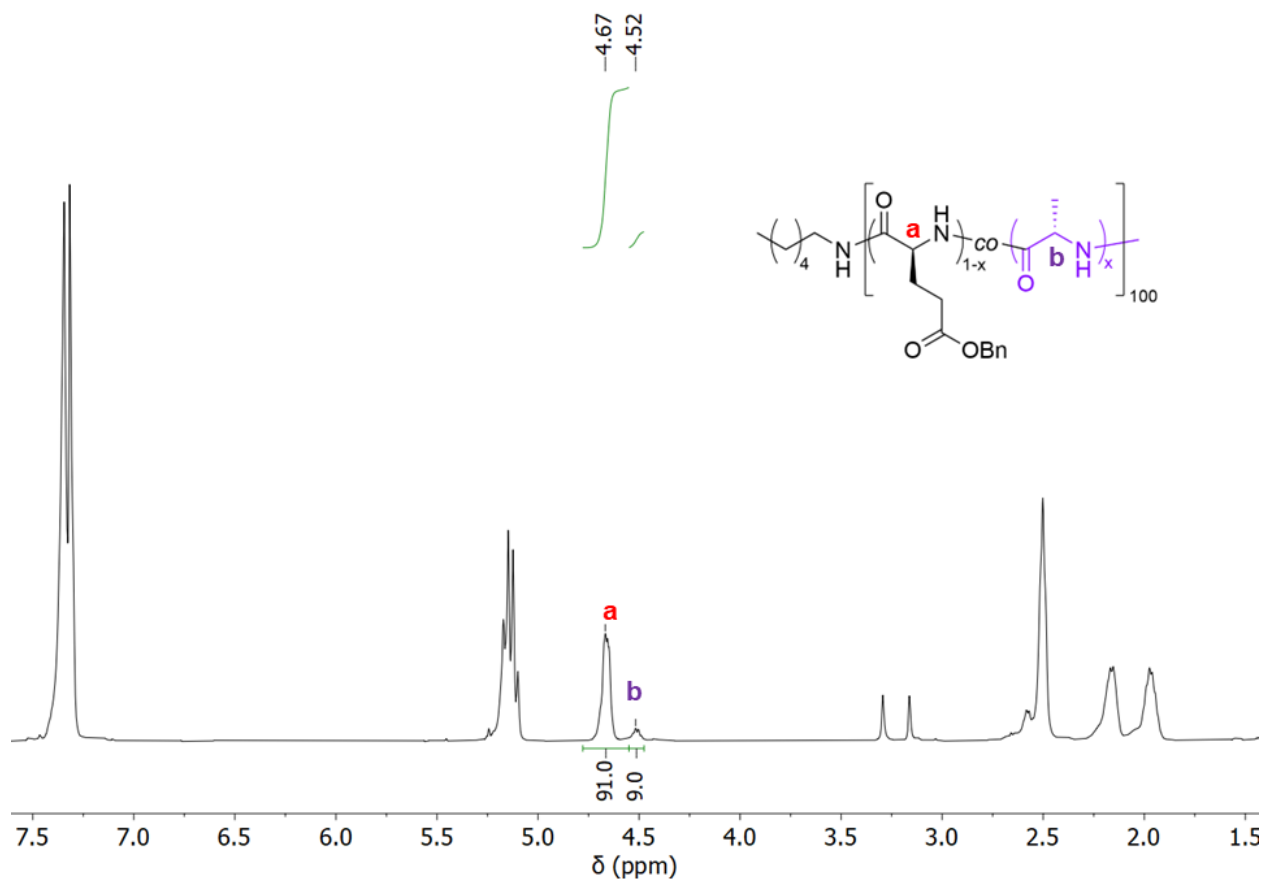


**Figure S41.**  $^1\text{H}$  NMR spectrum of  $\text{P}(\text{BLG}_{0.95}\text{-co-Ala}_{0.05})_{100}$  in  $\text{CDCl}_3/\text{TFA-}d$  (70:30, v/v).

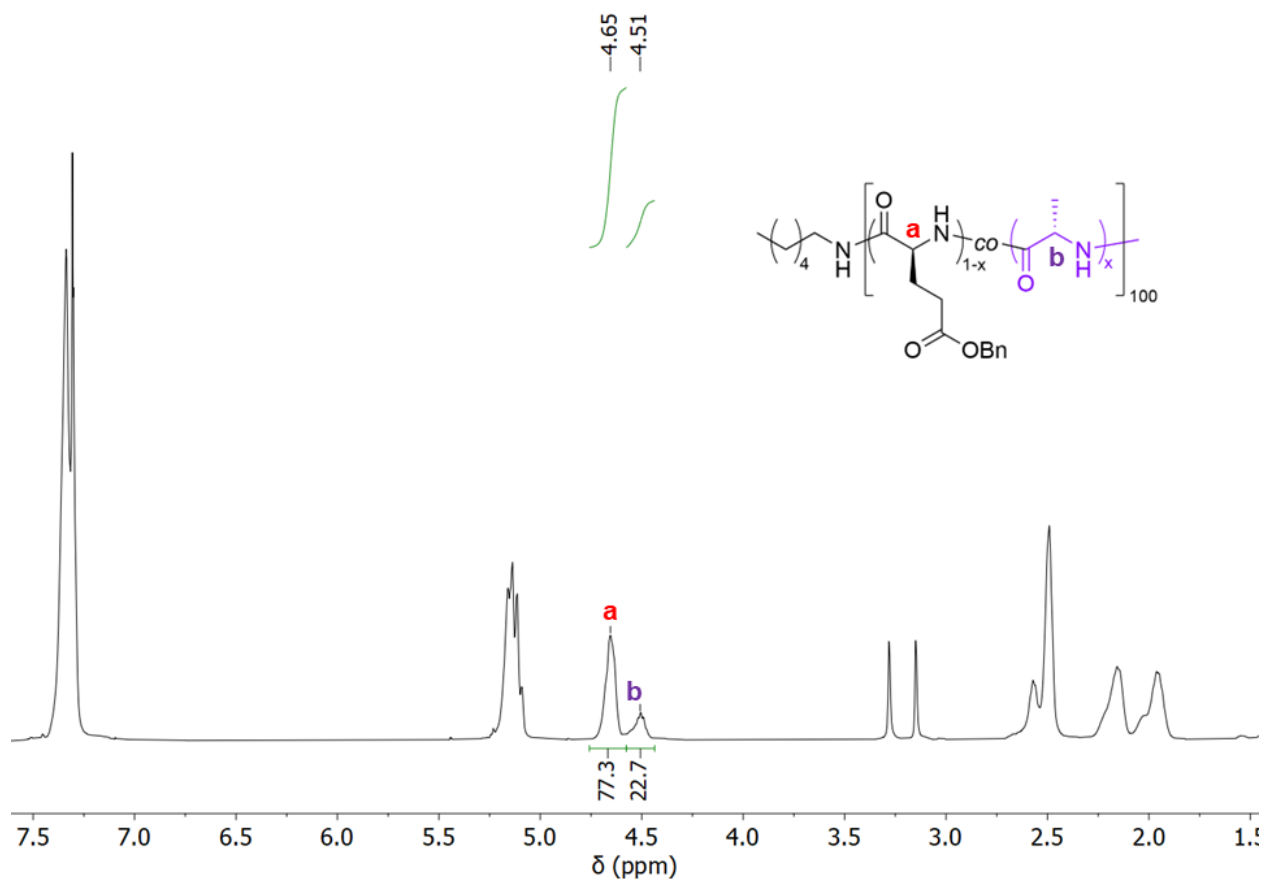


**Figure S42.**  $^1\text{H}$  NMR spectrum of  $\text{P}(\text{BLG}_{0.8}\text{-co-Ala}_{0.2})_{100}$  in  $\text{CDCl}_3/\text{TFA-}d$  (70:30, v/v).

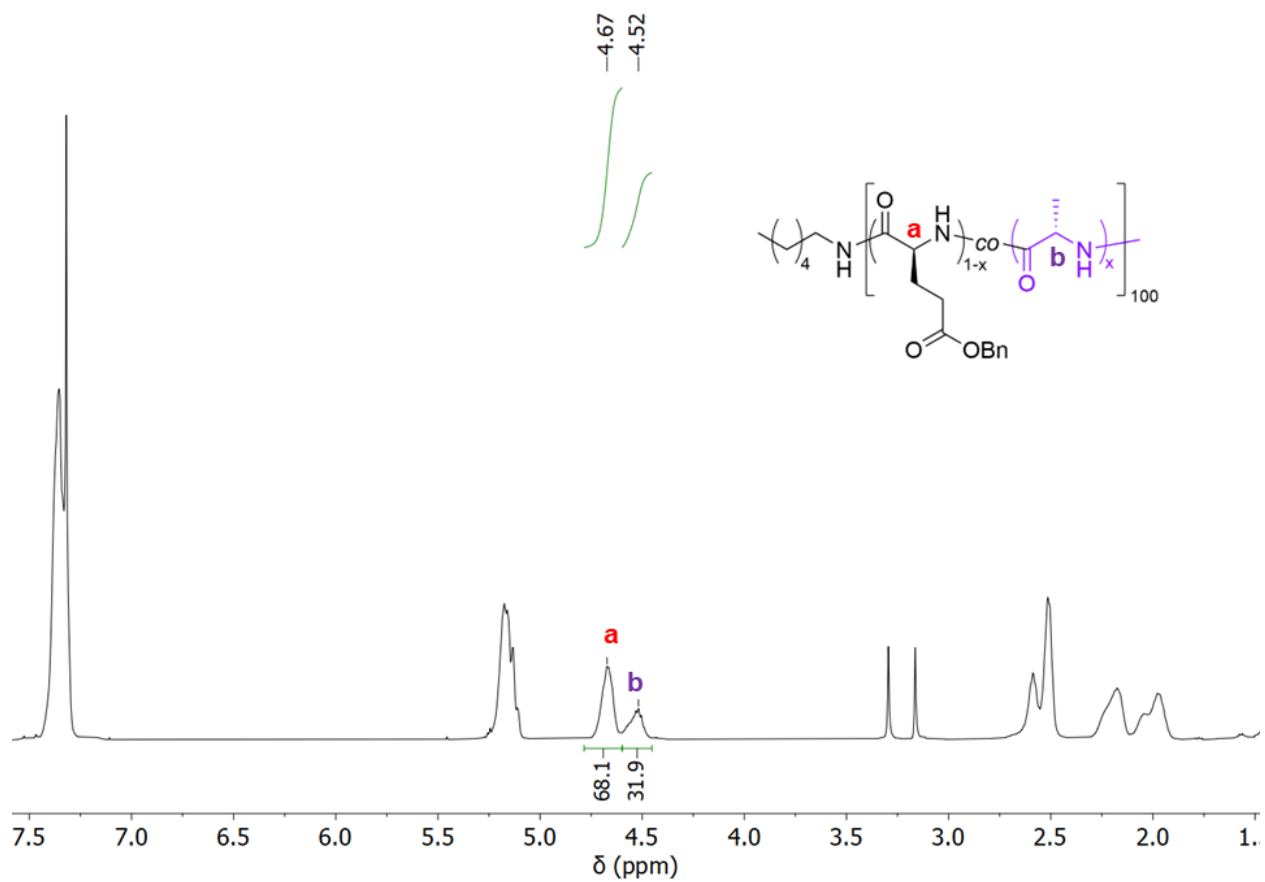


**Figure S43.** <sup>1</sup>H NMR spectrum of P(BLG<sub>0.7</sub>-co-Ala<sub>0.3</sub>)<sub>100</sub> in CDCl<sub>3</sub>/TFA-*d* (70:30, v/v).

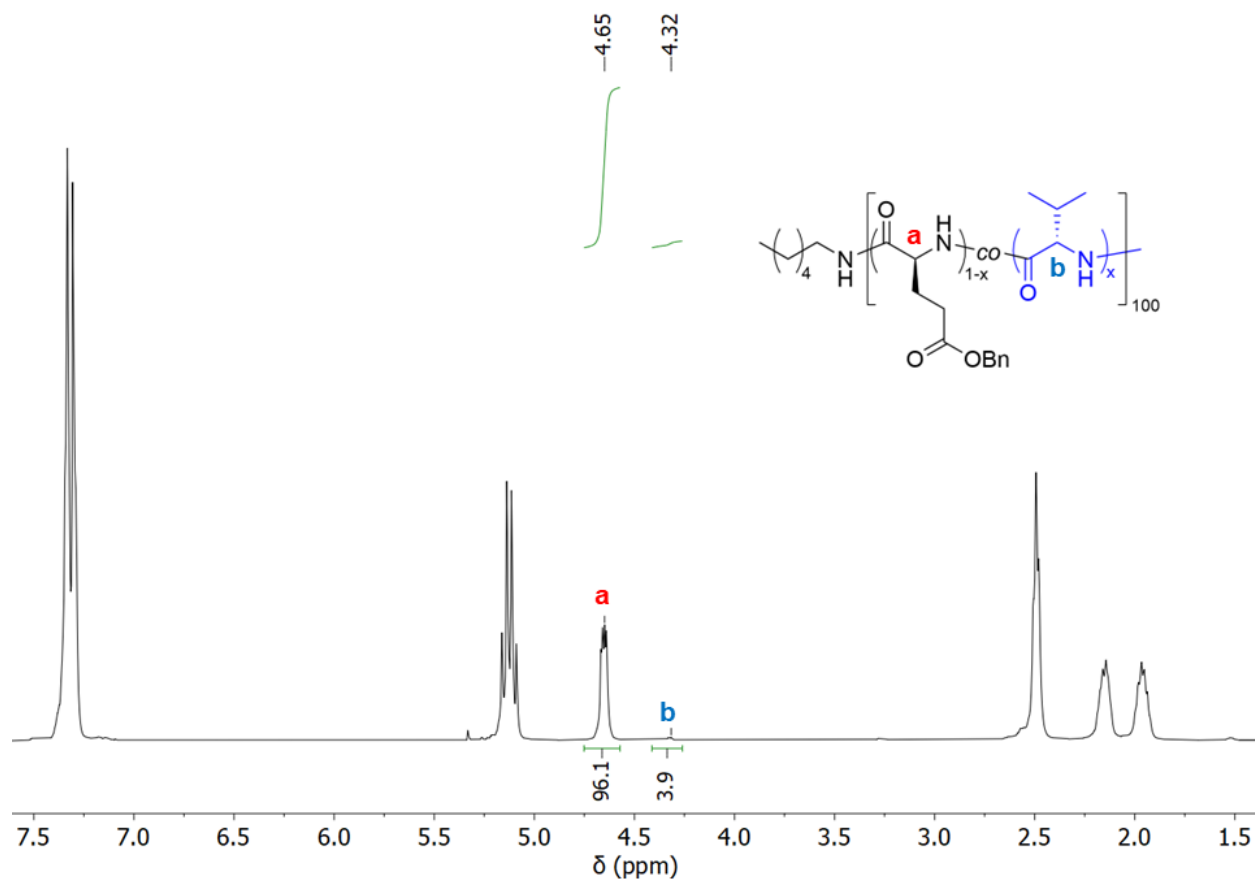


**Figure S44.**  $^1\text{H}$  NMR spectrum of  $\text{P}(\text{BLG}_{0.95}\text{-co-Val}_{0.05})_{100}$  in  $\text{CDCl}_3/\text{TFA-}d$  (70:30, v/v).

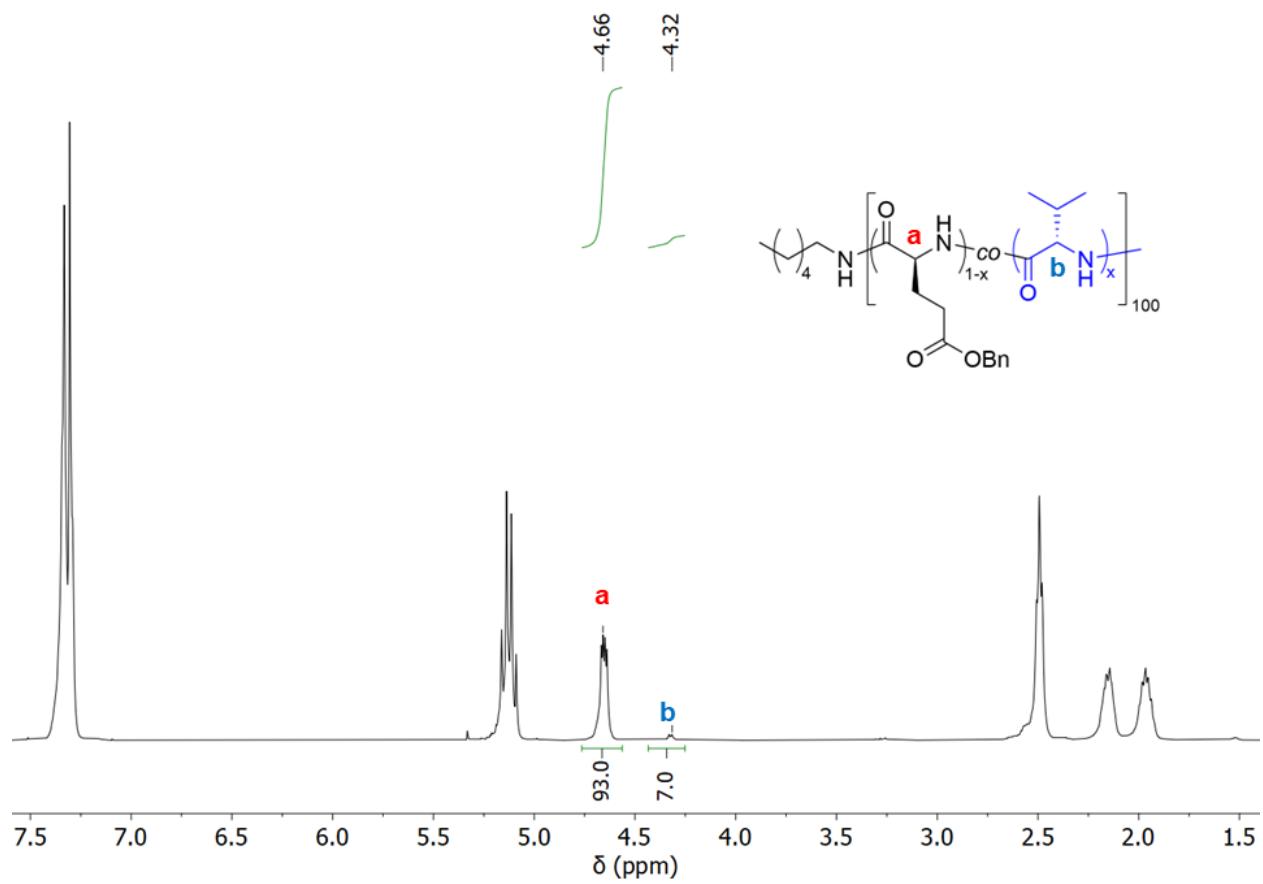


**Figure S45.**  $^1\text{H}$  NMR spectrum of  $\text{P}(\text{BLG}_{0.9}\text{-co-Val}_{0.1})_{100}$  in  $\text{CDCl}_3/\text{TFA-}d$  (70:30, v/v).

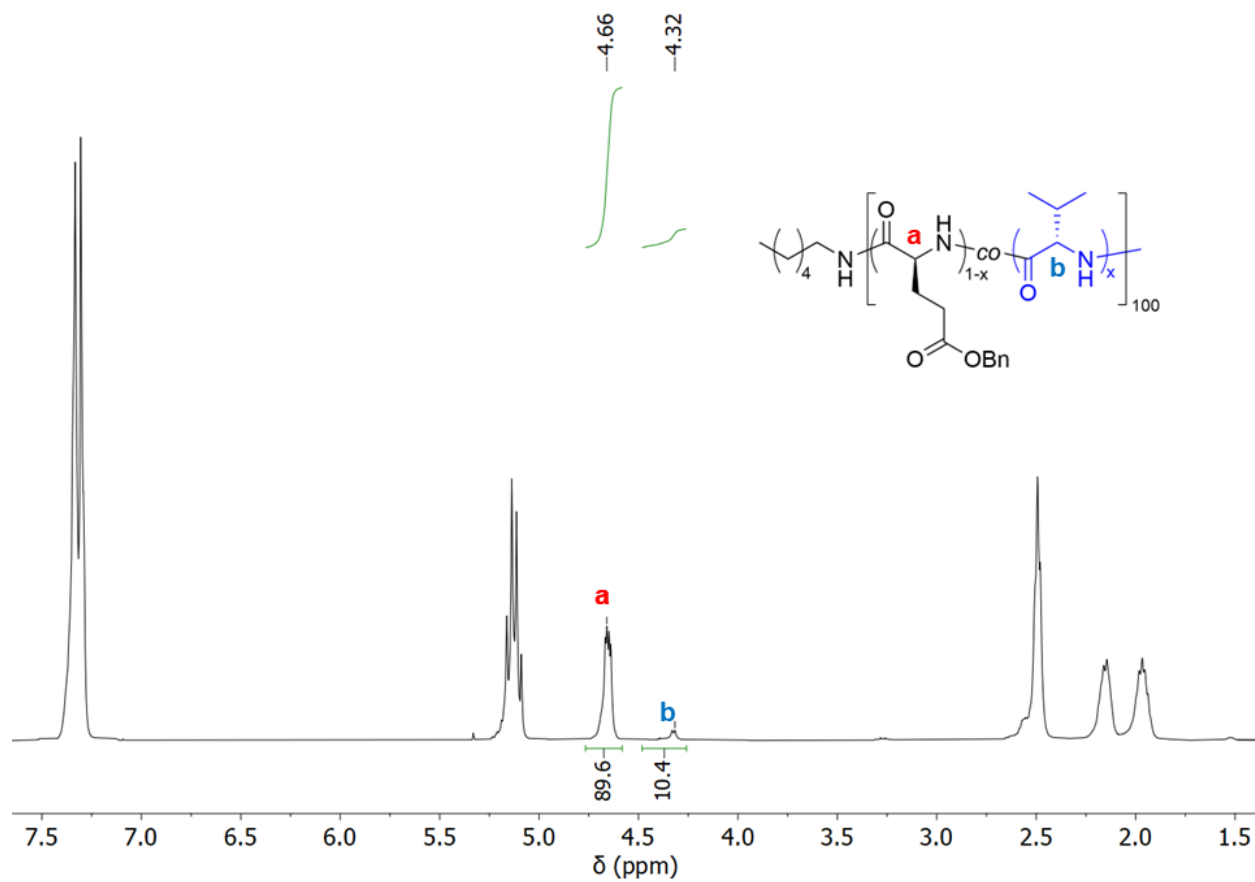


**Figure S46.**  $^1\text{H}$  NMR spectrum of  $\text{P}(\text{BLG}_{0.85}\text{-co-Val}_{0.15})_{100}$  in  $\text{CDCl}_3/\text{TFA-}d$  (70:30, v/v).

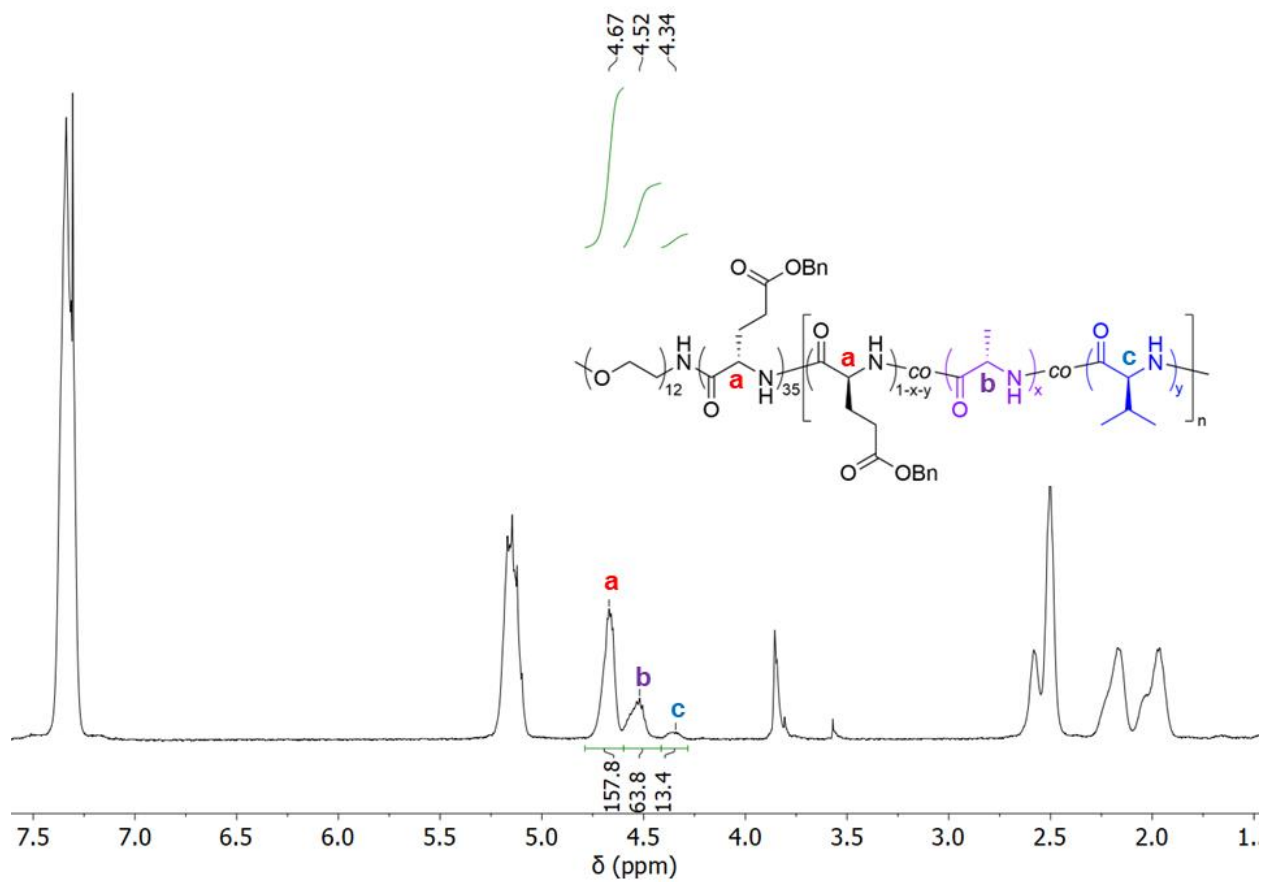


**Figure S47.**  $^1\text{H}$  NMR spectrum of PEG-polypeptide with  $\text{P}(\text{BLG}_{0.65}\text{-co-Ala}_{0.3}\text{-co-Val}_{0.05})_{200}$  in  $\text{CDCl}_3/\text{TFA-d}$  (70:30, v/v).

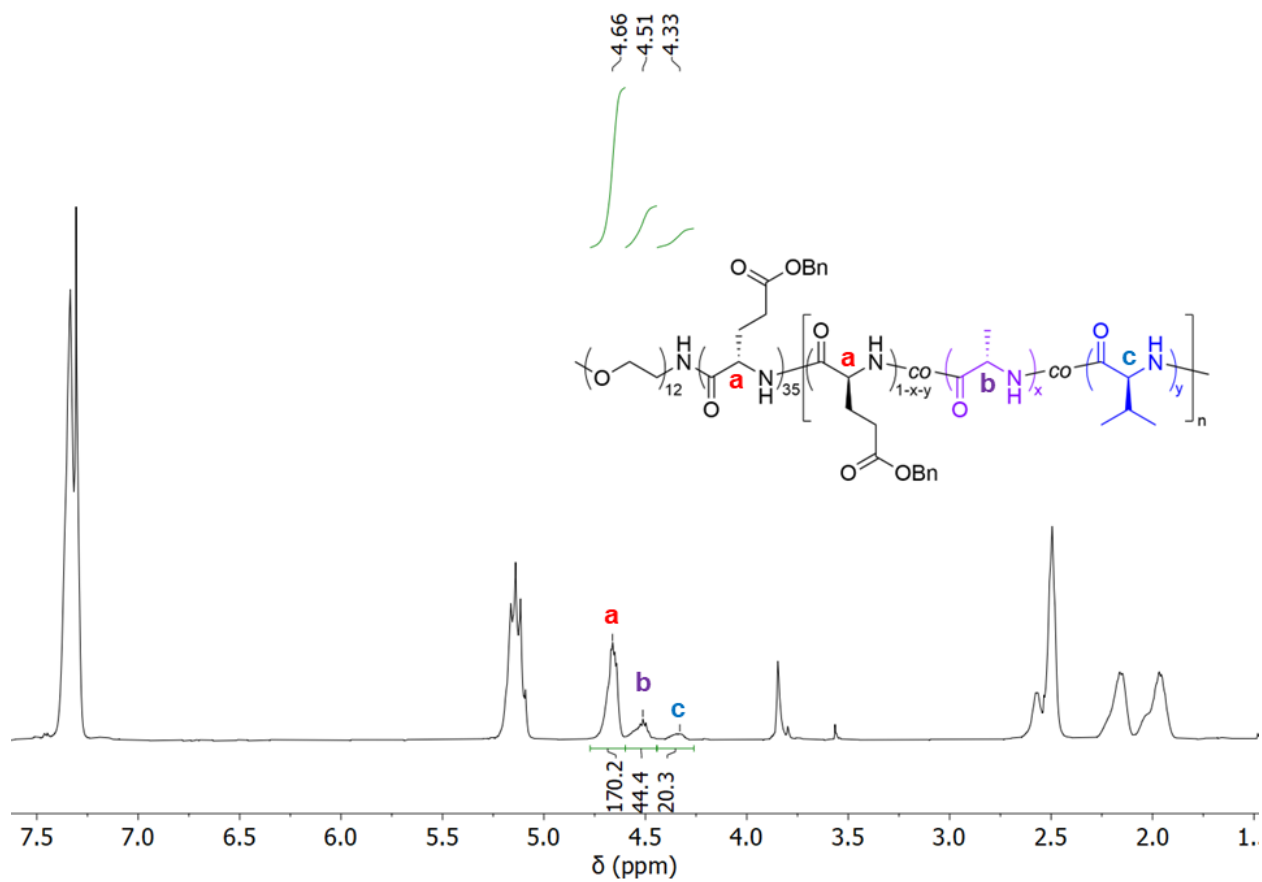


**Figure S48.**  $^1\text{H}$  NMR spectrum of PEG-polypeptide with P(BLG<sub>0.7</sub>-co-Ala<sub>0.2</sub>-co-Val<sub>0.1</sub>)<sub>200</sub> in  $\text{CDCl}_3/\text{TFA-d}$  (70:30, v/v).

## 6. References.

- (1) Song, Z.; Fu, H.; Wang, J.; Hui, J.; Xue, T.; Pacheco, L. A.; Yan, H.; Baumgartner, R.; Wang, Z.; Xia, Y.; Wang, X.; Yin, L.; Chen, C.; Rodríguez-López, J.; Ferguson, A. L.; Lin, Y.; Cheng, J. Synthesis of polypeptides via bioinspired polymerization of in situ purified N-carboxyanhydrides. *Proc. Natl. Acad. Sci. U. S. A.* **2019**, *116*, 10658-10663.
- (2) Holowka, E. P.; Pochan, D. J.; Deming, T. J. Charged polypeptide vesicles with controllable diameter. *J. Am. Chem. Soc.* **2005**, *127*, 12423-12428.
- (3) Habraken, G. J.; Peeters, M.; Dietz, C. H.; Koning, C. E.; Heise, A. How controlled and versatile is N-carboxy anhydride (NCA) polymerization at 0 °C? Effect of temperature on homo-, block-and graft (co) polymerization. *Polym. Chem.* **2010**, *1*, 514-524.
- (4) Chan, N. J.-A.; Gu, D.; Tan, S.; Fu, Q.; Pattison, T. G.; O'Connor, A. J.; Qiao, G. G. Spider-silk inspired polymeric networks by harnessing the mechanical potential of  $\beta$ -sheets through network guided assembly. *Nat. Commun.* **2020**, *11*, 1-14.
- (5) Yang, L. Using an in-vacuum CCD detector for simultaneous small-and wide-angle scattering at beamline X9. *J. Synchrotron Radiat.* **2013**, *20*, 211-218.
- (6) Bradbury, E.; Elliott, A.; Hanby, W. Optical rotatory dispersion and infrared studies of  $\beta$ -structures of poly-O-benzyl-L-serine in solution. *J. Mol. Biol.* **1962**, *5*, 487-496.
- (7) Mondeshki, M.; Spiess, H. W.; Aliferis, T.; Iatrou, H.; Hadjichristidis, N.; Floudas, G. Hierarchical self-assembly in diblock copolypeptides of poly ( $\gamma$ -benzyl-L-glutamate) with poly poly (L-leucine) and poly (O-benzyl-L-tyrosine). *Eur. Polym. J.* **2011**, *47*, 668-674.
- (8) Lu, H.; Cheng, J. Hexamethyldisilazane-mediated controlled polymerization of  $\alpha$ -amino acid N-carboxyanhydrides. *J. Am. Chem. Soc.* **2007**, *129*, 14114-14115.
- (9) Song, Z.; Fu, H.; Baumgartner, R.; Zhu, L.; Shih, K.-C.; Xia, Y.; Zheng, X.; Yin, L.; Chipot, C.; Lin, Y.; Cheng, J. Enzyme-mimetic self-catalyzed polymerization of polypeptide helices. *Nat. Commun.* **2019**, *10*, 5470.
- (10) Fu, H.; Baumgartner, R.; Song, Z.; Chen, C.; Cheng, J.; Lin, Y. Generalized model of cooperative covalent polymerization: connecting the supramolecular binding interactions with the catalytic behavior. *Macromolecules* **2022**, *55*, 2041-2050.
- (11) Xue, T.; Song, Z.; Wang, Y.; Zhu, B.; Zhao, Z.; Tan, Z.; Wang, X.; Xia, Y.; Cheng, J. Streamlined synthesis of PEG-polypeptides directly from amino acids. *Macromolecules* **2020**, *53*, 6589-6597.
- (12) Xia, Y.; Song, Z.; Tan, Z.; Xue, T.; Wei, S.; Zhu, L.; Yang, Y.; Fu, H.; Jiang, Y.; Lin, Y.; Lu, Y.; Ferguson, A. L.; Cheng, J. Accelerated polymerization of N-carboxyanhydrides catalyzed by crown ether. *Nat. Commun.* **2021**, *12*, 732.
- (13) Zelzer, M.; Heise, A. Determination of copolymerisation characteristics in the N-carboxy anhydride polymerisation of two amino acids. *Polym. Chem.* **2013**, *4*, 3896-3904.
- (14) Yang, T.; Benson, K.; Fu, H.; Xue, T.; Song, Z.; Duan, H.; Xia, H.; Kalluri, A.; He, J.; Cheng, J.; Lin, Y. Modeling and Designing Particle-Regulated Amyloid-like Assembly of Synthetic Polypeptides in Aqueous Solution. *Biomacromolecules* **2021**, *23*, 196-209.
- (15) Meisl, G.; Kirkegaard, J. B.; Arosio, P.; Michaels, T. C.; Vendruscolo, M.; Dobson, C. M.; Linse, S.; Knowles, T. P. Molecular mechanisms of protein aggregation from global fitting of kinetic models. *Nat. Protoc.* **2016**, *11*, 252-272.
- (16) Lee, N. H.; Frank, C. W. Surface-initiated vapor polymerization of various  $\alpha$ -amino acids. *Langmuir* **2003**, *19*, 1295-1303.
- (17) Koenig, J.; Sutton, P. Raman scattering of some synthetic polypeptides: Poly ( $\gamma$ -benzyl L-glutamate), poly-L-leucine, poly-L-valine, and poly-L-serine. *Biopolymers* **1971**, *10*, 89-106.
- (18) Fändrich, M.; Dobson, C. M. The behaviour of polyamino acids reveals an inverse side chain effect in amyloid structure formation. *EMBO J.* **2002**, *21*, 5682-5690.